RESEARCH MEMORANDUM

WIND-TUNNEL INVESTIGATION AT MACH NUMBERS OF 1.5 AND 2.0 OF A CANARD MISSILE CONFIGURATION

By J. Richard Spahr and Robert A. Robinson

Ames Aeronautical Laboratory
Moffett Field, Calif.

NATIONAL ADVISORY COMMITTEE
FOR AERONAUTICS

WASHINGTON

May 11, 1951

NATIONAL ADVISORY COMMITTEE FOR AERONAUTICS

RESEARCH MEMORANDUM

WIND-TUNNEL INVESTIGATION AT MACH NUMBERS OF 1.5 AND 2.0 OF A CANARD MISSILE CONFIGURATION

By J. Richard Spahr and Robert A. Robinson

SUMMARY

Wind-tunnel tests were performed at Mach numbers of 1.5 and 2.0 to investigate the force, moment, and control characteristics of a canard missile configuration (Grumman XSSM-N-6) and its components in both pitch and sideslip. The missile had small all-movable horizontal control surfaces at the nose and a cruciform wing at the rear, all of trapezoidal plan form. Trailing-edge flaps on the vertical fins were provided to supply directional control.

The results of the investigation showed no unsatisfactory aerodynamic characteristics in pitch or in sideslip for the complete configuration or for the various combinations of components tested. The complete configuration was longitudinally and directionally stable for the center of gravity located at the body midlength position, and the magnitude of the stability was essentially constant throughout the range of angle of attack (-2° to 8°) and sideslip (-8° to 2°) investigated.

Force, moment, and control-effectiveness values for the complete missile and its components were computed through the use of approximate theories, and comparisons with the experimental results are presented. For the body alone and in combination with either the wing or canard surfaces, the theoretical lift and moment curves were in reasonable agreement with the experimental results at both Mach numbers. For the complete missile, the predicted values of lift coefficient at both Mach numbers and the pitching-moment coefficients at $M = 1.5$ were also in reasonable agreement with the experimental results; whereas at $M = 2.0$ the pitching-moment coefficients were considerably less in magnitude than the experimental values. The lift effectiveness of the canard surfaces was overestimated at $M = 1.5$ by linear theory, whereas the moment effectiveness was considerably underestimated at both Mach numbers. The cross-force and yawing-moment effectiveness of the rudders were predicted within about 15 percent by linearized supersonic airfoil theory.

The complete configuration in sideslip at a positive angle of attack exhibited a positive dihedral effect which increased with positive deflections of the canard surfaces.

INTRODUCTION

In order to obtain a realistic prediction of the performance, stability, and control characteristics of a missile configuration, the interaction effects among the various components (wing, body, and tail) must be known. Both the theoretical and experimental aerodynamic characteristics of wings and bodies acting alone have been investigated rather extensively, but only limited results are available on the interaction among the components of wing-body-tail configurations. One means for assessing the applicability of existing information on these interaction effects is a correlation of the experimentally determined characteristics of particular missile configurations with the characteristics predicted from theoretical methods.

A wind-tunnel investigation has been made to measure the lift, drag, and static longitudinal- and directional-stability and control characteristics of the Grumman XSSM-N-6 (Rigel) Pilotless Aircraft at Mach numbers of 1.5 and 2.0 to correlate the experimental results with available theory where possible, and to ascertain from the experimental results whether or not some of the more important tactical and guidance requirements of the missile could be satisfied.

The Grumman XSSM-N-6 (Rigel) Pilotless Aircraft is a ram-jet powered, surface-to-surface missile of canard arrangement employing lifting surfaces of trapezoidal plan form. All-movable canard surfaces provide longitudinal control, and trailing-edge flaps (rudders) on the vertical fins supply directional control. The missile is designed to cruise at an altitude of 50,000 feet at a Mach number of 2.0 and to maneuver in an essentially unbanked attitude throughout its flight path. The canard surfaces are required to produce an acceleration of 3g in pitch at cruise conditions, and the rudders must supply the necessary directional control. The missile must be longitudinally and directionally stable with respect to the center of gravity at Mach numbers from 1.5 to 2.0, booster fins providing stability at Mach numbers below this range.

The present tests were conducted at the request of the Bureau of Aeronautics, U. S. Navy, and the model was furnished by the Grumman Aircraft Engineering Corporation.

NOTATION

All forces and moments are referred to the system of axes shown in figure 1.

a_n	normal acceleration, feet per second squared
C_D	drag coefficient $\left(\frac{\text{total drag} - \text{base drag}}{qS}\right)$
ΔC_D	rise in drag coefficient above minimum $\left(C_D - C_{D_{min}}\right)$
$C_{D_{min}}$	minimum drag coefficient
C_l	rolling-moment coefficient $\left(\frac{\text{rolling moment}}{qSd}\right)$
C_L	lift coefficient $\left(\frac{\text{lift}}{qS}\right)$
C_m	pitching-moment coefficient $\left(\frac{\text{pitching moment}}{qSd}\right)$
C_n	yawing-moment coefficient $\left(\frac{\text{yawing moment}}{qSd}\right)$
C_c	cross-force coefficient $\left(\frac{\text{cross force}}{qS}\right)$
d	maximum body diameter, inches
g	acceleration due to gravity, feet per second squared
h	pressure altitude, feet
l	body length, inches
q	free-stream dynamic pressure, pounds per square inch
M	Mach number
N.P.	neutral point aft of body nose, referred to maximum body diameter, d
R	Reynolds number, referred to body length, l

[redacted]

S	body frontal area, square inches
W	gross weight, pounds
α	angle of attack, degrees
β	angle of sideslip, degrees
ϵ	angle of downwash, degrees
δ_c	canard-surface angle, degrees
δ_r	rudder angle, degrees
η_w	wing efficiency, $\left[\frac{\left(\frac{dC_m}{d\alpha}\right)_{BHVC} - \left(\frac{dC_m}{d\alpha}\right)_{BC}}{\left(\frac{dC_m}{d\alpha}\right)_{BHV} - \left(\frac{dC_m}{d\alpha}\right)_{B}}\right]$

Configuration Designations

B	body
C	canard surfaces
H	horizontal wings
V	vertical fins

APPARATUS

Wind Tunnel and Balance

The Ames 1- by 3-foot supersonic wind tunnel No. 2, in which this investigation was conducted, is an intermittent-operation, nonreturn, variable-pressure wind tunnel. The compressed dry air supply is obtained from the Ames 12-foot pressure wind tunnel and is expanded from a maximum pressure of 6 atmospheres through the 1- by 3-foot nozzle to atmospheric pressure. The total pressure, and hence the Reynolds number, is controlled by means of a throttling valve. The wind tunnel is equipped with a variable Mach number nozzle having a rectangular test section 1 foot wide by approximately 3 feet high. The Mach number can be varied from about 1.2 to 4.0 by changing the shape of the flexible steel plates which form the upper and lower walls of the nozzle.

The strain-gage balance and other instrumentation used in these tests were essentially the same as those used in the Ames 1- by 3-foot supersonic wind tunnel No. 1. (See reference 1.) Pitching or yawing moments were measured by strain gages mounted on the model supporting sting, and the rolling moments were measured by means of strain gages incorporated in the balance. A drawing of the strain-gage balance and model support is presented in figure 2.

Model and Support

The configuration tested (fig. 3) was a model of a ram-jet powered canard missile having a 40° conical shock diffuser. For this model the duct inlet was faired over, and hence there was no internal flow through the model. The body had a fineness ratio of 11.5 and terminated in a short, tapered boattail section. All wings and control surfaces had trapezoidal plan forms and were removable to allow model build-up tests. The canard surfaces had a 6-percent-thick double-wedge section, and the wing and fin had a 6-percent-thick hexagonal section. (See fig. 3(d).) The angles of the all-movable canard surfaces were set by machined incidence blocks which were held in place by cover plates. Small gaps (about 0.001-inch wide), which increased with control deflection, existed between the root section of the canard surfaces and the body. These gaps were left unsealed for the present tests. Fixed rudder deflections were built into interchangeable vertical fins, resulting in no gap at the hinge line or at the rudder-body juncture. The geometric characteristics of the wings and controls are summarized in table I.

The model was supported by a straight sting inserted into the model base at an angle of 3°. This arrangement, shown in figure 4, enabled the model to be tested through an angle-of-attack range of -2° to 8°, an angle-of-sideslip range of -8° to 2°, and an angle-of-sideslip range of -5° to 5° at an angle of attack of 3°. The model was mounted with the plane of the wing vertical for the sideslip tests.

The sting support was shielded from aerodynamic forces by a shroud that extended to within a small distance (about 1/32 inch) of the base of the model. Static-pressure orifices in the sting adjacent to the base of the model permitted measurement of the base pressure of the body. Unpublished pressure-distribution results have shown that the pressures thus obtained are in close agreement with the average pressures acting over the base.

ANALYSIS OF DATA

The measured results have been reduced to aerodynamic coefficients which are referred to the axis system shown in figure 1. The angle of attack or sideslip of the model was computed from the sum of the balance-angle setting, the inclination of the model relative to the balance under no load, and the change in angle due to the support and balance deflection under aerodynamic loading. The latter quantity was determined from the predetermined elastic properties of the balance and model-support system and from the measured forces and moments. The control-surface angles were measured directly, prior to the test runs, and it was estimated that the change in these angles due to aerodynamic loading was negligible.

Corrections to Experimental Results

The aerodynamic coefficients presented have been corrected for the effects of wind-tunnel-stream nonuniformities. Corrections were made to the force and moment coefficients for the loading induced on the body at each angle of attack or sideslip by the stream-angle variations and by the static-pressure gradients. A description of the method used in calculating these corrections is given in the appendix of reference 2. The corrections for the effect of stream angle on the loading over the lifting surfaces were computed on the basis of the average chordwise value of stream angle since the variation over the chords of the individual wings was small. The effects of the vertical pressure gradients on the horizontal surfaces were negligible by virtue of the small thicknesses involved.

[redacted]

All drag data have been corrected to a common pressure on the base equal to the free-stream static pressure. Thus, the drag data presented represent the fore drag or the difference between the total drag and the base drag.

Precision of Results

The estimated error in the experimental results for a given test condition is taken as the square root of the sum of the squares of the uncertainties in each of the measured quantities and in the calculated corrections for the nonuniform stream conditions. The following table lists the estimated errors at both Mach numbers and at an angle of attack of 8° or an angle of sideslip of −8°:

Quantity	Estimated error	
	Configurations B and BC	Configurations BHV and BHVC
C_L and C_c	±0.03	±0.04
C_m and C_n	±.08	±.19
C_D	±.01	±.01
C_l	--	±.004
M	±.02	±.02
α (deg)	±.08	±.08
δ (deg)	--	±.06

[redacted]

TESTS AND RESULTS

Tests were performed for the following model configurations and conditions:

Configuration	M	α	β	δ_c	δ_r	Measurements
B, BC, BHV, and BHVC	1.5 and 2.0	-2° to 8°	0°	0°	0°	C_L, C_D, and C_m
BHVC	1.5 and 2.0	-2° to 8°	0°	$-5^\circ, 0^\circ, 5^\circ, 10^\circ$, and 15°	0°	C_L, C_D, and C_m
BHVC	1.5 and 2.0	0°	-8° to 2°	0°	0° and -20°	C_c, C_D, and C_n
BHVC	2.0	3°	-5° to 5°	$0^\circ, 5^\circ$, and 10°	0°	C_c, C_D, C_n, and C_l

The average Reynolds number for these tests was 8.0 million based on the model length.

The experimental results for the various configurations tested in pitch are presented in figures 5 to 12 and the results for the complete missile tested in sideslip are given in figures 13 and 14. Theoretical lift and moment curves are also shown where possible for comparison with the corresponding experimental results. A summary of both the experimental and theoretical characteristics of the several missile components and combinations is presented in table II. The experimental slopes represent the values in the vicinity of zero angle of attack or sideslip.

DISCUSSION

Characteristics in Pitch

Configuration B.- The lift, moment, and drag results for the body are presented in figure 5. It is observed that with increasing angles

of attack the lift-curve slope $dC_L/d\alpha$ characteristically increases, whereas the moment-curve slope $dC_m/d\alpha$ decreases. From these effects it is apparent that a rearward shift of the center of pressure occurs with increasing angles of attack since the center-of-pressure travel is essentially equal to changes in the ratio of the moment to the lift.

Theoretical curves for the lift, moment, and drag characteristics of the body are shown in figure 5 as computed from the potential-flow theory of reference 3 and from the theory of reference 4 in which the potential-flow theory is modified to account for the aerodynamic loading induced by the viscous cross flow over the body. The drag coefficients termed theoretical in figure 5 represent the sum of the experimental minimum drag coefficient and the rise in drag coefficient with increase in angle of attack ΔC_D obtained from these two theories.

A comparison of the results presented in figure 5 shows that the lift coefficients and changes in the drag coefficients computed by the method of reference 4 are in considerably closer agreement with the experimental results than are those computed by the method of reference 3. A similar agreement was found in references 4 and 5 for a wide variety of bodies at subsonic and supersonic velocities. It is noted that the pitching-moment coefficients for the two theories are nearly coincident. This result follows from the fact that the center of the viscous cross force is near the midlength point of the body, which is the point to which the pitching moments are referred. The experimental values of pitching-moment coefficient at high angles of attack are noted to be somewhat less than the theoretical values at $M = 2.0$ but the agreement is close at $M = 1.5$.

Configurations BC and BHV.- The lift, moment, and drag results for the body in combination with the canard surfaces and with the horizontal wings and vertical fins are presented in figures 6 and 7, respectively. It is noted that with the exception of configuration BC at $M = 1.5$ the lift and moment curves for these configurations are essentially linear, indicating little center-of-pressure change with increasing angle of attack. The lift curve of configuration BC at $M = 1.5$ (fig. 6(a)) exhibits an increase in slope $dC_L/d\alpha$ with an increase in angle of attack similar to that shown by the body alone (fig. 5).

Theoretical lift and moment curves (figs. 6 and 7) for configurations BC and BHV have been computed by means of a modified slender-body theory and a body-upwash theory for compairson with the experimental results. With both of these methods, the lift and moment coefficients for a wing-body combination at a given angle of attack are taken as the sum of the theoretical lift or moment coefficient for the body and the corresponding value for the wing in combination with a semi-infinite cylinder having a diameter equal to that of the body at the wing location. For the present applications the theoretical

[redacted]

lift and moment characteristics of the body for both methods were obtained from the theory of reference 4, which includes the aerodynamic loading due to the viscous cross flow over the body. It was assumed in these calculations, however, that no viscous cross force existed over the portion of the body which contained wings or canard surfaces, and that the effect of the canard surface or wing downwash on the body was negligible. It was also assumed that the vertical fins had no effect on the lift or moment characteristics of configuration BHV in pitch.

For the modified slender-body theory, the lift and moment coefficients for a wing-cylinder combination are taken as those computed by the slender-wing-body theory of reference 6 multiplied by the ratio of the wing lift and moment coefficients obtained from linear theory to the corresponding coefficients obtained from the slender-wing theory of reference 7. The linear-theory characteristics for the wing and canard surfaces of the present configuration were obtained from reference 8. A discussion of the development of the modified slender-body theory and its application to triangular-wing and body combinations are given in reference 2 wherein good agreement is shown with the experimental results.

For the body-upwash theory, the lift and moment coefficients for a wing-cylinder combination are given by the lift and moment coefficients of the exposed wing operating in the theoretical flow field of an inclined cylinder. These wing characteristics are obtained by means of strip theory, that is, the integration over the plan form of the product of the local angle of attack $(\alpha-\epsilon)$ and the local rate of change of load coefficient with angle of attack as computed from linear theory for a flat wing of the given plan form. These lift and moment coefficients may be expressed by the general equations

$$C_L = \frac{1}{S} \iint_T \frac{d(\Delta p/q)}{d\alpha} (\alpha-\epsilon)\, dxdy$$

$$C_m = \frac{1}{Sd} \iint_T \frac{d(\Delta p/q)}{d\alpha} (\alpha-\epsilon)\, xdxdy$$

where

S reference area

$\frac{\Delta p}{q}$ local load coefficient

[redacted]

ϵ local downwash angle

d reference length

x streamwise distance forward of moment reference point

y spanwise distance from body axis

τ exposed wing or canard surfaces

For a circular cylinder, the theoretical upwash distribution in the horizontal meridian plane (z=0) is given by the relationship (reference 9)

$$-\epsilon = \alpha\left(\frac{a}{y}\right)^2$$

where

a body radius

The theoretical load coefficients $\Delta p/q$ for the present plan forms were obtained from reference 8. Applications of the body-upwash theory to wings of simple plan forms in combination with a semi-infinite cylinder and comparisons with experimental results are given in references 10 and 11. Closed expressions are derived in reference 10 for the lift characteristics of a combination having a general trapezoidal plan-form wing, and the lift and pitching-moment characteristics of a body in combination with rectangular or triangular wings are given in reference 11. Generally good agreement is shown in these reports with experimental results.

Comparison of the results for configuration BC (fig. 6) shows that the theoretical lift and moment coefficients are in good agreement with the experimental values, the results computed by the body-upwash theory being generally in closer conformity with experiment than those from the modified slender-body theory. For configuration BHV (fig. 7), however, it is noted that the theoretical values of lift computed by both theories are less than the experimental values and that the moments are more positive than the experimental values. In contrast to the comparison for configuration BC, the results for configuration BHV computed by the modified slender-body theory are generally in closer agreement with the experimental results than those computed by the body-upwash theory.

Although the lift and moment results computed from the two theoretical methods are in reasonable agreement with each other, such agreement may be fortuitous because of the assumptions and approximations involved

in these methods. It is believed that the modified slender-body theory is inherently a more valid method than the body-upwash method since, in the former method, both the effect of the wing on the body and of the body on the wing are included whereas, in the latter method, it is assumed that the interference is confined to the effect of the body flow field on the wing and that no wing lift is carried over onto the body, which is contrary to experimental evidence. Moreover, in the body-upwash method it is assumed that no interaction takes place between adjacent lifting elements on the wing as induced by the local body-upwash field. This assumption is valid only in regions of small spanwise velocity gradients. However, the actual spanwise downwash gradients are relatively large, especially over the inboard region of the wing. The results of calculations by means of the linearized lifting-surface theory indicate that the local loadings induced on a wing by the body flow field are considerably less in this region than those predicted by strip theory. It follows that the lift computed by this method is underestimated by neglecting the effect of the wing on the body and is overestimated by using strip theory. Hence, these two approximations apparently result in nearly compensating effects on the lift and moment coefficients of the present configuration.

Configuration BHVC.- The lift, moment, and drag results for the complete configuration are presented in figure 8. It is noted that the lift curves are essentially linear and that the variation of the moment-curve slope with angle of attack is small. Thus, no appreciable change in static longitudinal stability occurred over the range of angle of attack investigated. The neutral-point locations given in table II indicate an increase in stability with Mach number.

As a measure of the interference effects of the canard surfaces and body on the wing-body combination, the pitching-moment results of configurations B, BC, BHV, and BHVC can be combined to determine the wing efficiency η_w as defined in NOTATION. The wing efficiency is influenced principally by the downwash field behind the canard surfaces and body and secondarily by the differences in the Mach number and dynamic pressure at the wing from the free-stream values. The resulting values of η_w, given in table II, were computed from the average slopes of the experimental pitching-moment curves. These values indicate that the net interference effect is relatively small since a value of 1 represents no interference. These relatively high wing efficiencies are probably due to the fact that the effect on the wing load of the downwash behind the canard surfaces inboard of the canard tips is largely compensated by the effect of the upwash behind the surfaces outboard of the tips since the wing span is considerably greater than the span of the canard surfaces. Schlieren photographs are presented in figure 9 which show side and plan views of the vortex wake shed by the canard surfaces and wing. From the plan view it is observed that the tip vortices converge in passing downstream, indicating a rolling

[redacted]

up of the vortex sheet. From an analysis of these schlieren photographs it was found that the canard–surface tip vortices are essentially rolled up in the vicinity of the wings. This result is in qualitative agreement with reference 12.

Since the interference effects of the canard surfaces and body on the wing–body combination were found to be small, as indicated by the experimental values of η_w (table II), theoretical lift and moment curves for the complete configuration have been computed on the basis of zero interference (η_w=1) between the front and rear lifting surfaces. The results obtained from both the modified slender–body and body–upwash theories are shown in figure 8, and the lift– and moment–curve slopes at zero angle of attack from the modified slender–body theory are given in table II. The comparison between the theoretical and experimental results is generally similar to that shown for configuration BHV. This would be expected since the wings furnish the predominating influence on the characteristics of the complete configuration by virtue of their size and lift effectiveness.

The effects of deflection of the canard surfaces on the aerodynamic characteristics of the complete configuration are shown in figures 8 and 10. From figure 10, it is noted that the control–effectiveness parameters $dC_L/d\delta_c$ and $dC_m/d\delta_c$ are essentially constant over the angle–of–attack range and are independent of the control deflection except that at M = 1.5 the moment effectiveness decreased somewhat above about 6°. Theoretical lift and moment control–effectiveness values have been computed from linear theory (reference 8) on the assumption that the net interference effect on the wing is negligible. The results of these calculations are given in table II and figure 10. The lift results appear to be in reasonable agreement but the theoretical moment effectiveness $dC_m/d\delta_c$ is considerably less than the experimental values at both Mach numbers.

From the lift and moment results of figure 8, the maneuverability and stability characteristics of the missile for various conditions of flight can be estimated. Figure 11 shows the lift for zero pitching moment attainable with various control deflections with the center of gravity located at the midbody position. The corresponding normal accelerations for the design missile loading and for two altitudes are also shown. These accelerations are inversely proportional to the loading and, hence, values at other loadings may be determined accordingly. It is noted that with the larger control deflections the maneuverability increases with increases in Mach number and that a large decrease occurs with increases in altitude. A tactical requirement of the present missile is that an acceleration of 3g shall be developed at M = 2.0 at an altitude of 50,000 feet. Figure 11 indicates that a control deflection in excess of 15° would be required to meet this condition. Figure 12 shows the variation in normal acceleration with

[redacted]

static margin, which is an indication of the effect of static stability on maneuverability. For a constant control deflection it is noted that large reductions in the available accelerations are suffered by increases in the static margin, particularly in the region of low stability. The reduction of the static margin to permit large accelerations with a given control deflection, however, is accompanied by an increase in the angle of attack. In order to maintain large lift–drag ratios, it is desirable to avoid high angles of attack. The variation in acceleration with static margin for an angle of attack of 5° is shown in figure 12. It is noted that the acceleration increases slightly with increasing stability although, of course, larger control deflections are required to develop these accelerations.

Characteristics in Sideslip

The cross–force, yawing–moment, and drag results for configuration BHVC at zero angle of attack are presented in figure 13 as functions of angle of sideslip. Both the cross–force and yawing–moment curves are essentially linear indicating constant static directional stability over the test range of sideslip angles.

Theoretical values for the cross–force and yawing–moment curve slopes were computed by the two methods previously discussed for configurations BC and BHV in pitch. In these calculations it was assumed that the canard surfaces and horizontal wing had no effect on the cross–force and yawing–moment characteristics in sideslip. These theoretical results, given in figure 13 and table II, show that the cross–force coefficients are generally lower than the experimental values, the agreement being within 10 percent for the slender–body theory and only 20 percent for the body–upwash theory. The theoretical yawing–moment coefficients, however, are much less negative than the experimental values. This comparison is qualitatively similar to the previously discussed comparison for configuration BHV in pitch.

The effect of rudder deflection on the characteristics in sideslip is shown in figure 13. A rudder deflection of 20° results in an essentially constant increment of cross–force and yawing–moment coefficients over the sideslip range. Theoretical values for the rudder–effectiveness parameters $dC_c/d\delta_r$ and $dC_n/d\delta_r$ have been computed from linear theory and the results are tabulated in table II with the corresponding experimental values $\Delta C_c/\Delta\delta_r$ and $\Delta C_n/\Delta\delta_r$. Comparison of these results shows that the theoretical and experimental values are in close agreement except for the moment effectiveness $\Delta C_n/\Delta\delta_r$ at M = 2.0 which differs by about 15 percent.

The cross-force, yawing-moment, rolling-moment, and drag results for configuration BHVC at M = 2.0 and at 3° angle of attack are presented in figure 14 as functions of angle of sideslip for various canard-surface angles. The side-force and yawing-moment curves are essentially linear indicating that no changes in static directional stability occurred over the test range. Comparison of the side-force and yawing-moment curves for zero canard-surface angle and 3° angle of attack with those for an angle of attack of 0° (fig. 13) shows that both the side-force and yawing-moment curve slopes are reduced slightly due to an increase in angle of attack. (See table II.) The results presented in figure 14 show that increasing the canard-surface deflection also caused a reduction in these quantities and resulted in a destabilizing effect. The rolling-moment curves show that a positive dihedral effect occurred which increased with increasing canard-surface angles. The rolling moments encountered by this configuration in combined pitch and sideslip are probably caused by several factors. One of these factors is the interaction between the wings and vertical fins. Under these conditions, a difference in the flow field over the upper fin from that over the lower exists due to the inclination of the horizontal wing and, hence, when the vertical fin is inclined in sideslip, a differential loading over the fins results. A similar and compensating effect of the fins on the wing loads is experienced, but the resulting rolling moment for a rotationally symmetric configuration will be zero only when the angle of attack and sideslip are equal. A theoretical treatment for this effect is given in reference 13. For horizontal wings of different size or plan form or in a different longitudinal location from the vertical fins, a net rolling moment will be experienced at all combinations of angle of attack and sideslip. Another cause of these rolling moments is the effect of the asymmetric downwash distribution from the canard surfaces on the wing load distribution. This effect would be intensified by deflection of the canard surfaces and is probably the cause for the variation in rolling moment with control deflection shown in figure 14.

CONCLUDING REMARKS

Wind-tunnel tests were performed at Mach numbers of 1.5 and 2.0 to investigate the lift, drag, and longitudinal- and lateral-stability and control characteristics of a canard missile configuration. The results showed that the force and moment characteristics in pitch and sideslip were regular and that no appreciable change in static stability occurred over the test range of angle of inclination or of control-surface deflection. It was found that the lift and moment characteristics of the body alone and in combination with the wing or canard surfaces could be predicted reasonably well by existing theory. For the complete missile, the predicted values of lift coefficient at both Mach numbers and the

pitching-moment coefficients at M = 1.5 were in reasonable agreement with the experimental results; whereas at M = 2.0 the pitching-moment coefficients were considerably less in magnitude than the experimental values. The lift effectiveness of the canard surfaces was overestimated at M = 1.5 but predicted closely at M = 2.0 by linear theory; whereas the moment effectiveness was greatly underestimated at both Mach numbers. The cross-force and yawing-moment effectiveness of the rudders was predicted within 15 percent by linearized supersonic airfoil theory. The complete configuration in sideslip at a positive angle of attack exhibited positive dihedral effect which increased with increasing positive deflections of the canard surfaces.

Ames Aeronautical Laboratory,
National Advisory Committee for Aeronautics,
Moffett Field, Calif.

REFERENCES

1. Van Dyke, Milton D.: Aerodynamic Characteristics Including Scale Effect of Several Wings and Bodies Alone and in Combination at a Mach Number of 1.53. NACA RM A6K22, 1946.

2. Nielsen, Jack N., Katzen, Elliott D., and Tang, Kenneth K.: Lift and Pitching-Moment Interference Between a Pointed Cylindrical Body and Triangular Wings of Various Aspect Ratios at Mach Numbers of 1.50 and 2.02. NACA RM A50F06, 1950.

3. Munk, M. M.: The Aerodynamic Forces on Airship Hulls. NACA Rep. 184, 1924.

4. Allen, H. Julian: Estimation of the Forces and Moments Acting on Inclined Bodies of Revolution of High Finess Ratio. NACA RM A9I26, 1949.

5. Allen, H. Julian, and Perkins, Edward W.: Characteristics of Flow Over Inclined Bodies of Revolution. NACA RM A50L07, 1950.

6. Spreiter, John R.: Aerodynamic Properties of Slender Wing-Body Combinations at Subsonic, Transonic, and Supersonic Speeds. NACA TN 1662, 1948.

7. Jones, Robert T.: Properties of Low-Aspect-Ratio Pointed Wings at Speeds Below and Above the Speed of Sound. NACA Rep. 835, 1946. (Formerly TN 1032).

8. Lagerstrom, P. A., Wall, D., and Graham, M. E.: Formulas in Three-Dimensional Wing Theory (1). Douglas Rep. SM-11901, July 1946.

9. Beskin, L.: Determination of Upwash Around a Body of Revolution at Supersonic Velocities. Johns Hopkins Univ., APL/JHU CM-251, May 27, 1946.

10. Stewart, Homer J., and Meghreblian, Robert V.: Body-Wing Interference in Supersonic Flow. CIT JPL Prog. Rep. 4-99, June 2, 1949.

11. Dorrance, W. H.: Body-Tail Interference in Supersonic Flow Including an Example Application. Univ. of Mich., UMM-38, Aug. 1949.

12. Spreiter, John R., and Sacks, Alvin H.: The Rolling Up of the Trailing Vortex Sheet and its Effect on the Downwash Behind Wings. Jour. Aero. Sci., vol. 18, no. 1, Jan. 1951, pp. 21-32.

13. Maple, C. G., and Synge, J. L.: Aerodynamic Symmetry of Projectiles. Quart. of Applied Math., vol. 6, no. 4, Jan. 1949, pp. 345-366.

[redacted]

TABLE I.- DIMENSIONS OF EXPOSED WINGS AND CONTROL SURFACES

Quantity	Horizontal wings	Canard surfaces	Vertical fins	Rudder
Surface areas, in.^{2}	3.045	0.345	1.800	0.456
Aspect ratio	2.95	2.50	2.66	- - -
Taper ratio	.46	.50	.50	.50
Thickness ratio	.06	.06	.06	- - -
Leading-edge sweepback	14.0°	28.1°	20.5°	0°
Semispan, in.	1.531	.488	1.095	1.095
Mean aerodynamic chord, in.	1.063	.385	.851	.213

[redacted]

TABLE II.- SUMMARY OF RESULTS

Aerodynamic Characteristics in Pitch

Configuration	M	Lift		Moment			Drag		η_w
		$\frac{dC_L}{d\alpha}$	$\frac{dC_L}{d\delta_c}$	$\frac{dC_m}{d\alpha}$	$\frac{dC_m}{d\delta_c}$	N.P.	$\frac{\Delta C_D}{C_L^2}$	$C_{D_{min}}$	
B	1.5	0.035 (.028)	--	0.210 (.195)	--	--	--	0.40	--
	2.0	.042 (.028)	--	.190 (.196)	--	--	--	.35	--
BC	1.5	.078 (.083)	--	.375 (.384)	--	--	.041	.41	--
	2.0	.076 (.065)	--	.293 (.321)	--	--	.071	.35	--
BHV	1.5	.367 (.330)	--	-.520 (-.461)	--	--	.050	.58	--
	2.0	.288 (.240)	--	-.344 (-.266)	--	--	.067	.48	--
BHVC	1.5	.391 (.385)	.018 (.022)	-.256 (-.272)	.137 (.084)	6.40 (6.44)	.049	.59	.88
	2.0	.311 (.277)	.015 (.015)	-.235 (-.141)	.072 (.057)	6.51 (6.22)	.055	.49	1.00

Aerodynamic Characteristics in Sideslip
[Configuration BHVC]

M	α	δ_c	Cross-force		Moment			Drag	
			$\frac{dC_c}{d\beta}$	$\frac{\Delta C_c}{\Delta\delta_r}$	$\frac{dC_n}{d\beta}$	$\frac{\Delta C_n}{\Delta\delta_r}$	$\frac{dC_l}{d\beta}$	$\frac{\Delta C_D}{C_c^2}$	$C_{D_{min}}$
1.5	0°	0°	-0.245 (-.219)	0.031 (.034)	0.250 (.217)	-0.089 (-.089)	0	0.072	0.59
2.0	0°	0°	-.208 (-.161)	.021 (.023)	.180 (.090)	-.069 (-.059)	0	.012	.49
	3°	0°	-.195	--	.178	--	-.0030	.109	.55
		4.8°	-.188	--	.140	--	-.0091	--	.56
		9.8°	-.185	--	.100	--	-.0183	--	.59

Note: The values in parentheses are theoretical results corresponding to the experimental results directly above.

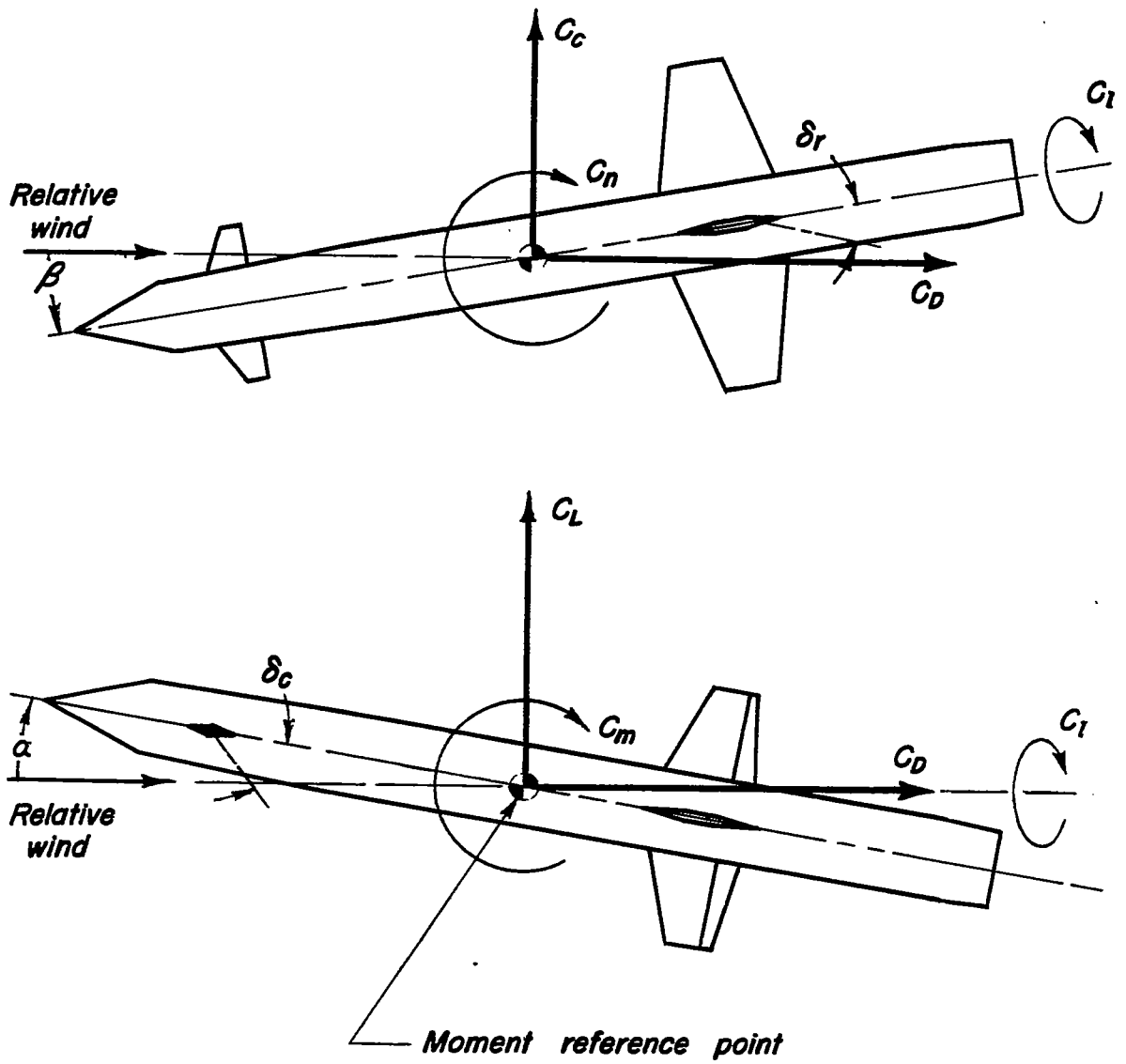

Figure 1. —Coordinate axis system and positive direction of forces, moments, and angles.

[redacted]

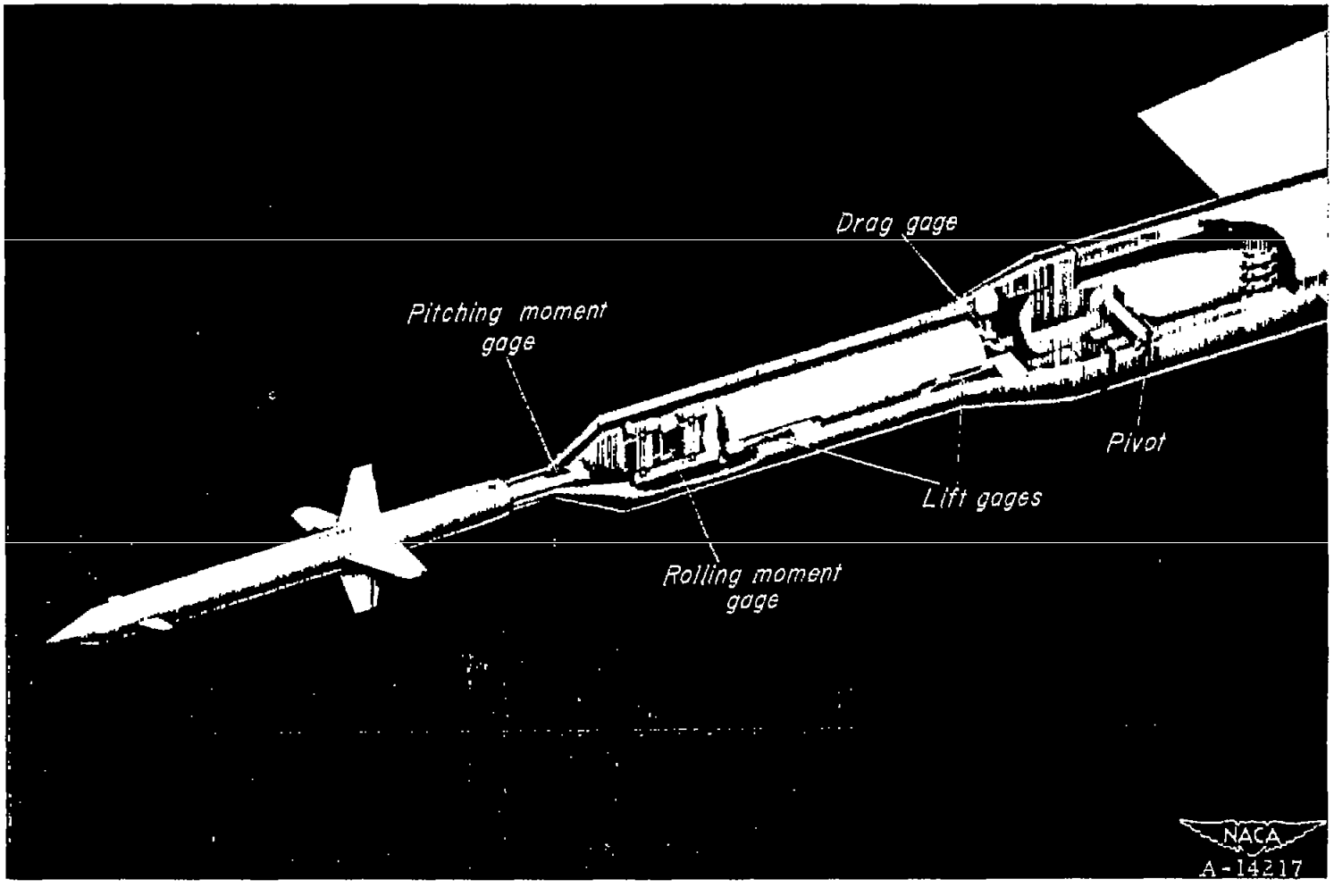

Figure 2.- Model support and strain-gage balance.

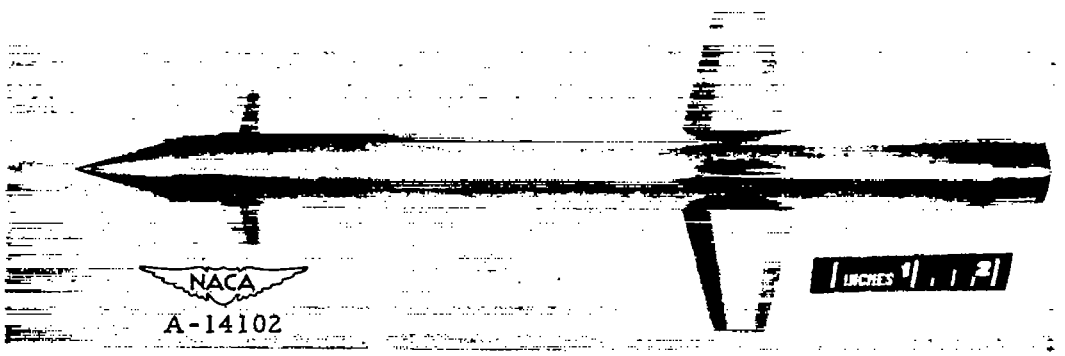

(a) Plan view.

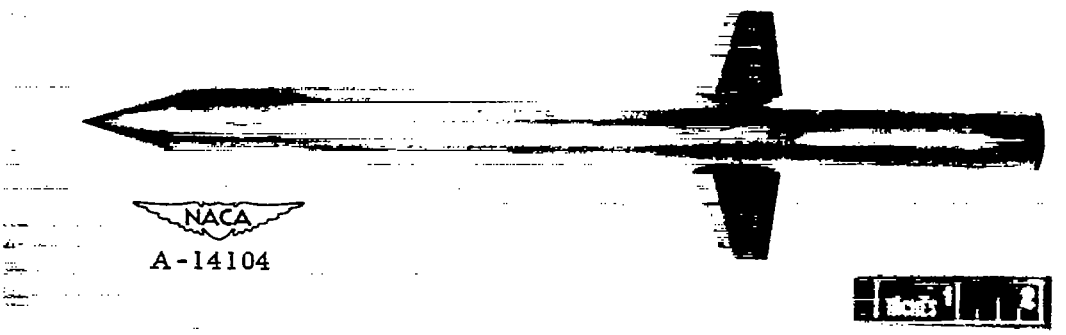

(b) Side view.

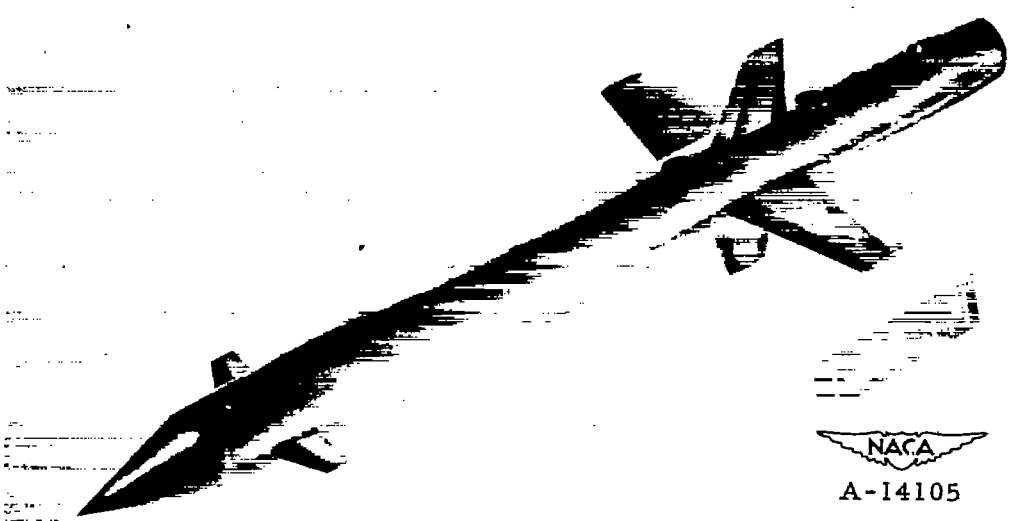

(c) Three-quarter view.

Figure 3.- Model configuration.

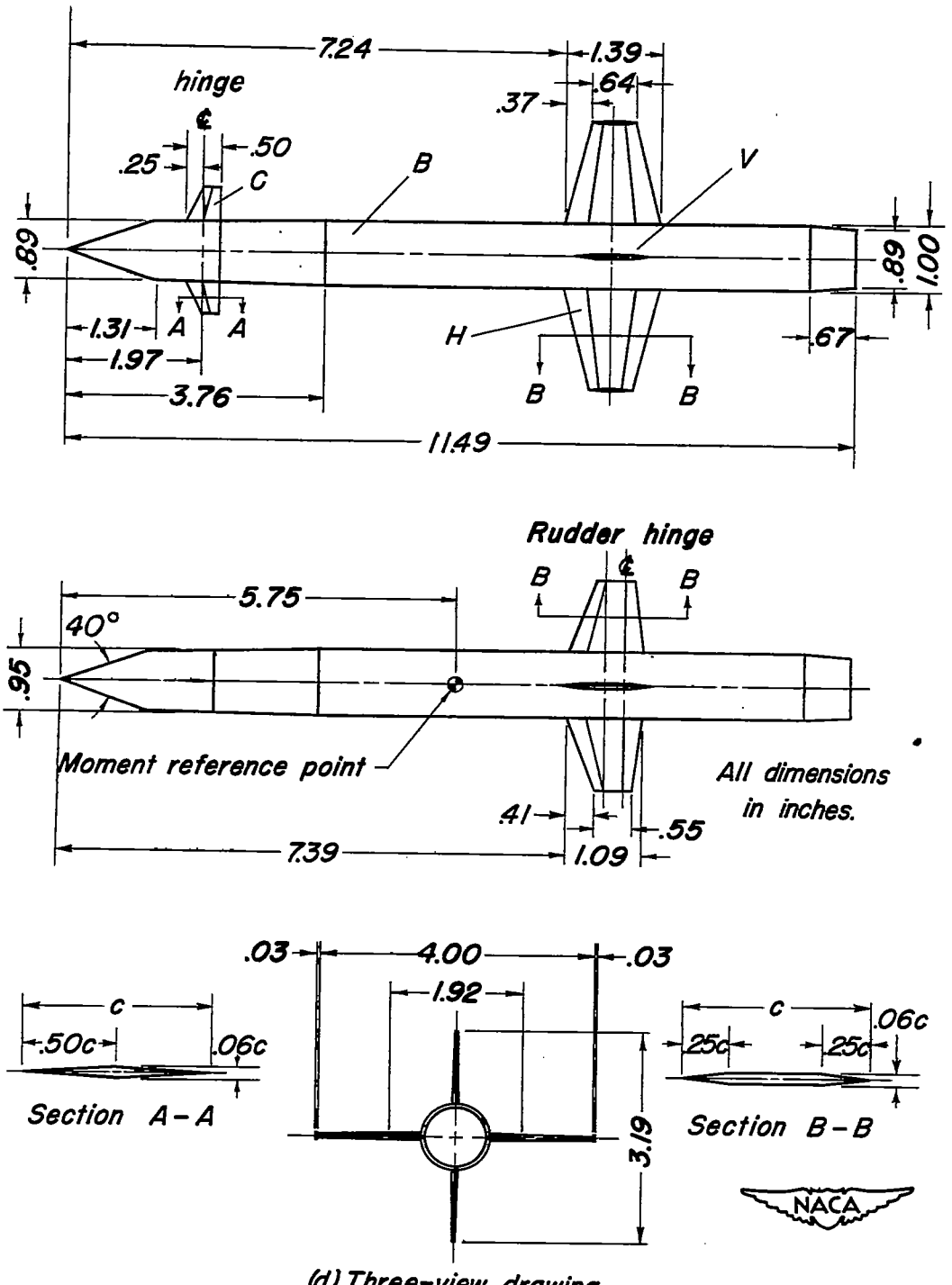

(d) Three-view drawing.

Figure 3.- Concluded.

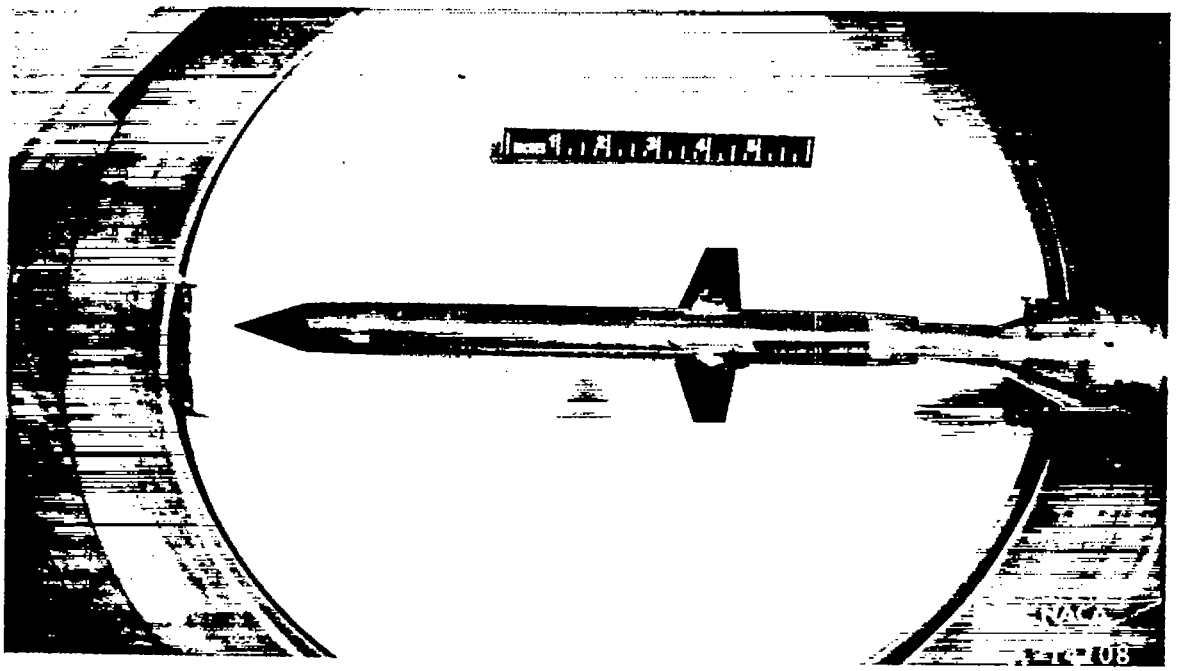

(a) Pitch tests.

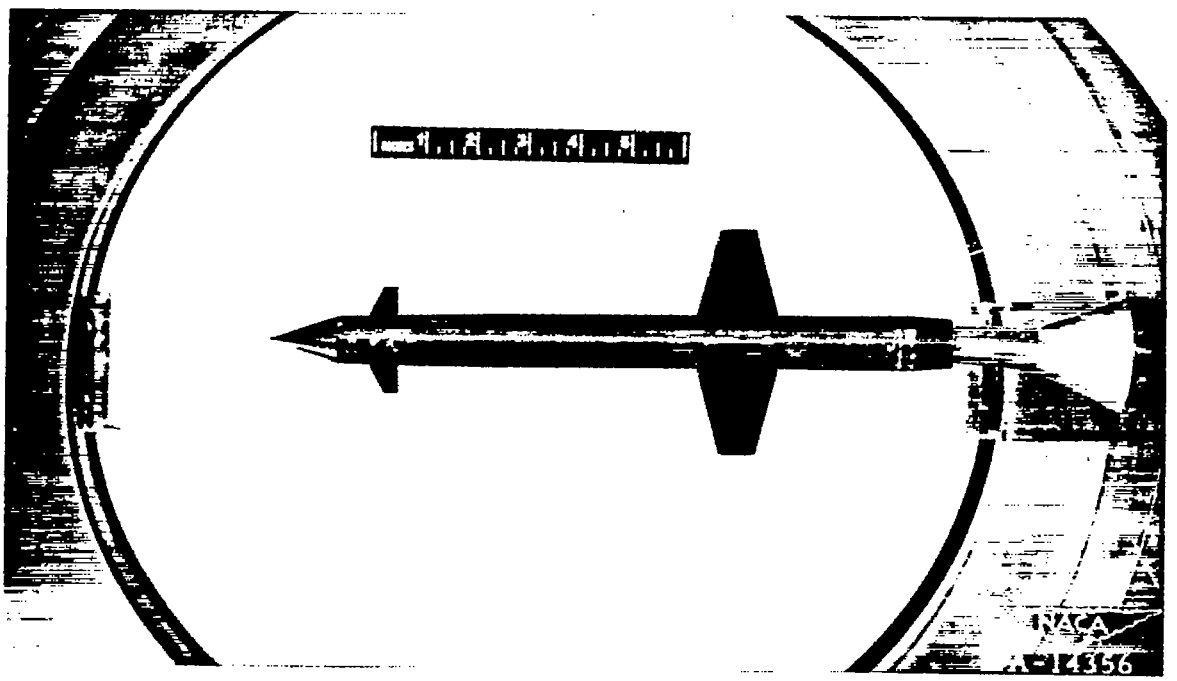

(b) Sideslip tests.

Figure 4.— Model installation in the wind tunnel.

[redacted]

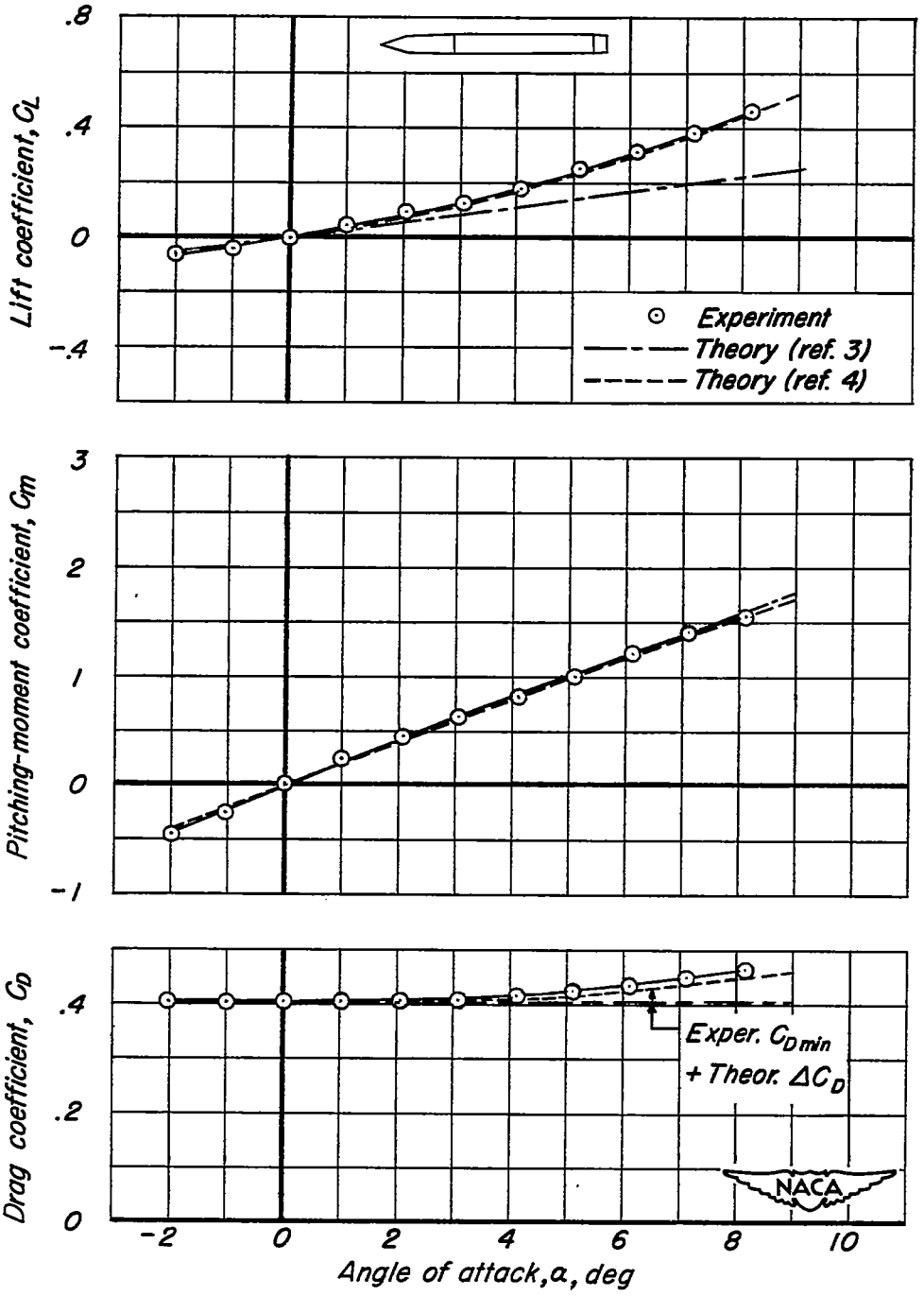

(a) $M = 1.5$

Figure 5.—Variation of lift, pitching-moment, and drag coefficients with angle of attack, configuration B.

[redacted]

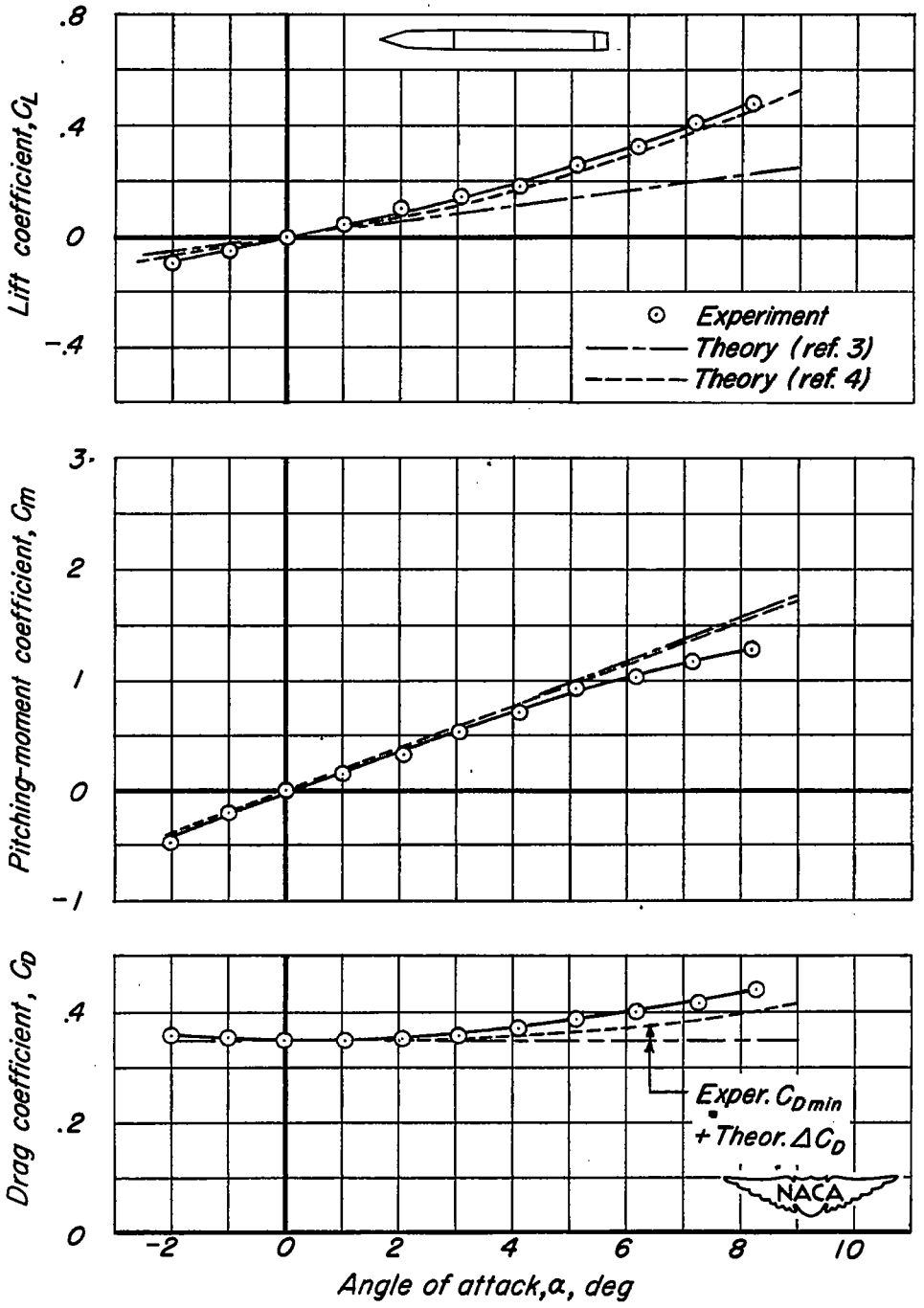

(b) M = 2.0

Figure 5.- Concluded.

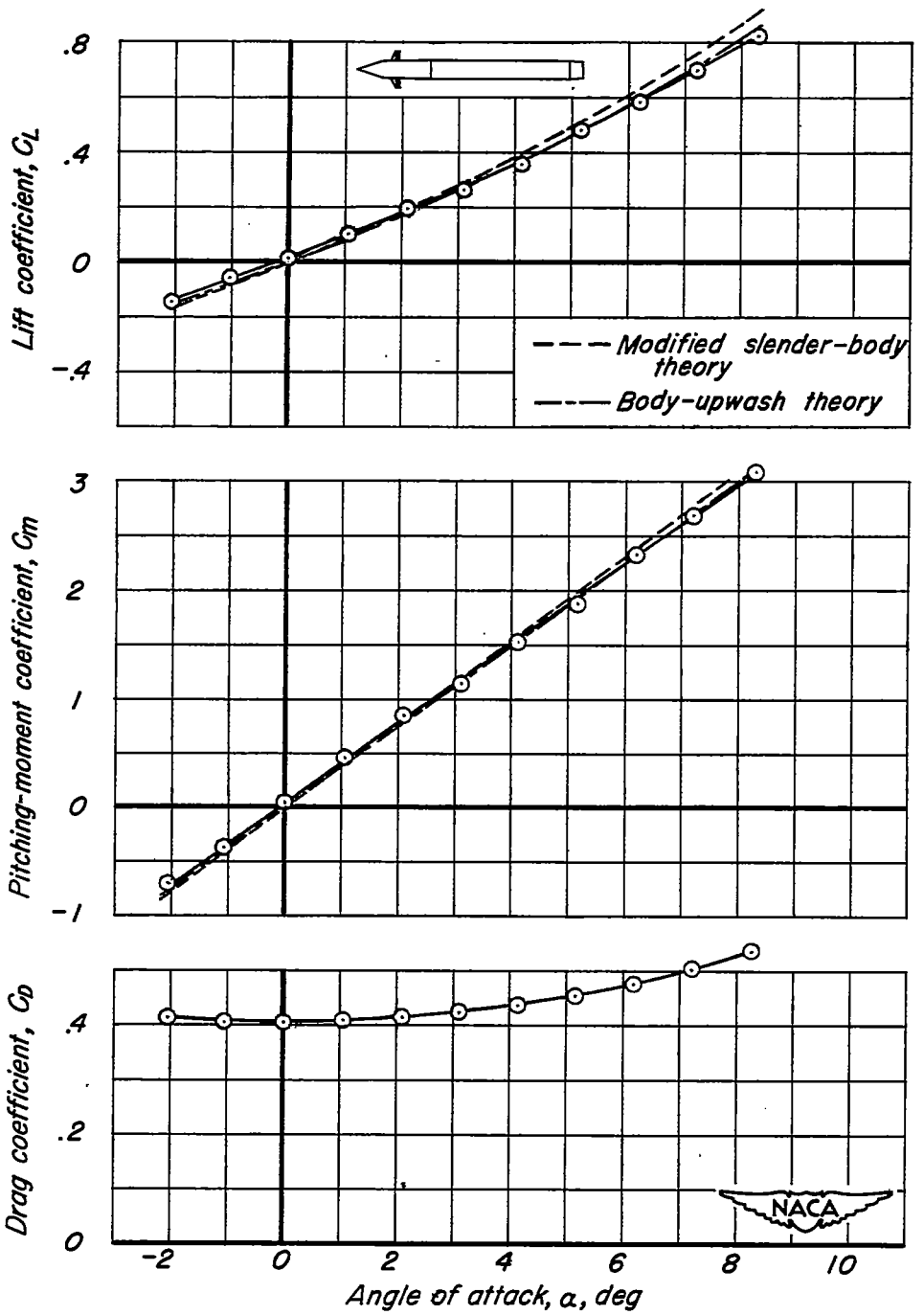

(a) $M = 1.5$

Figure 6.—Variation of lift, pitching-moment, and drag coefficients with angle of attack, configuration BC.

[redacted]

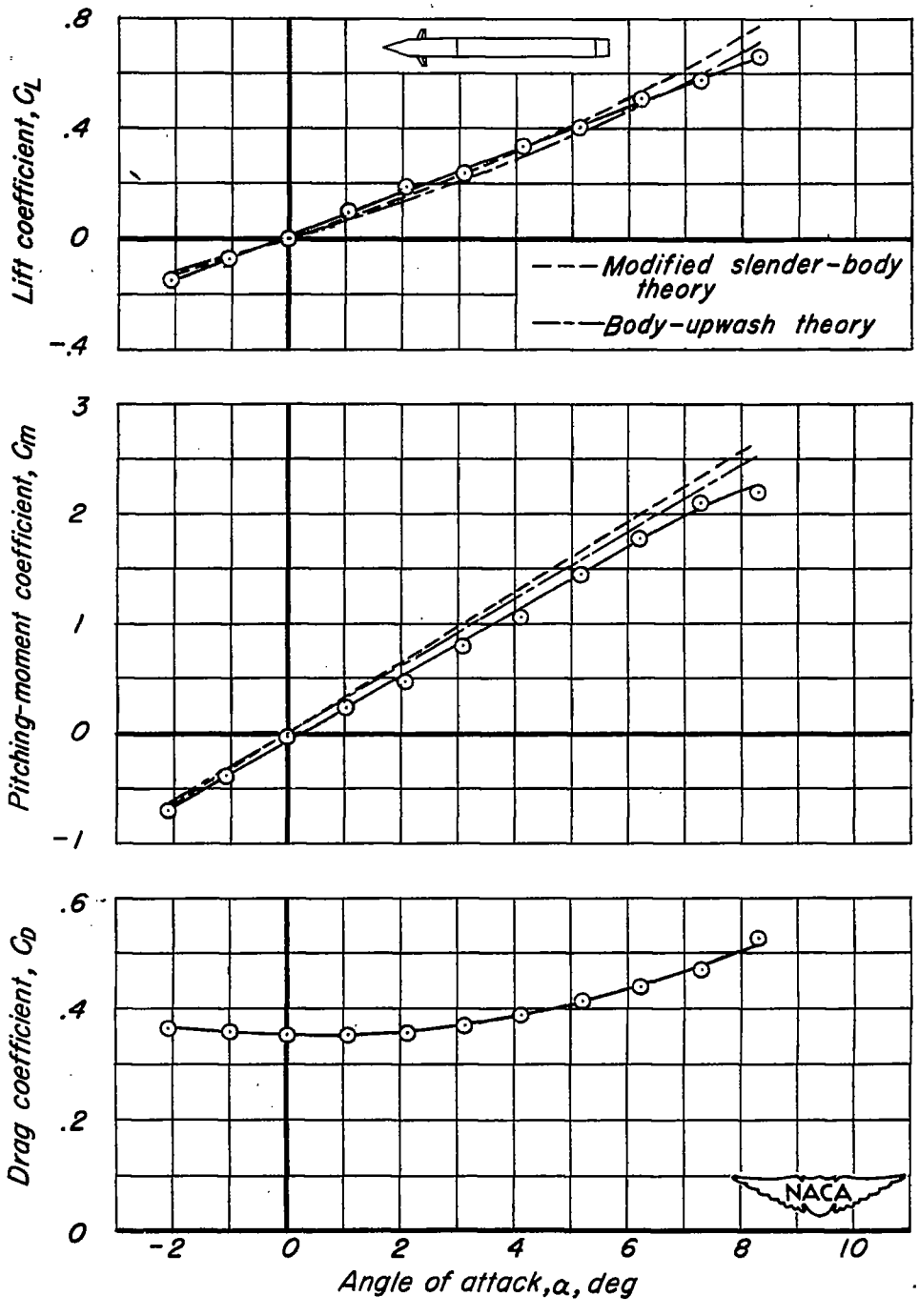

(b) M = 2.0

Figure 6.- Concluded.

[redacted]

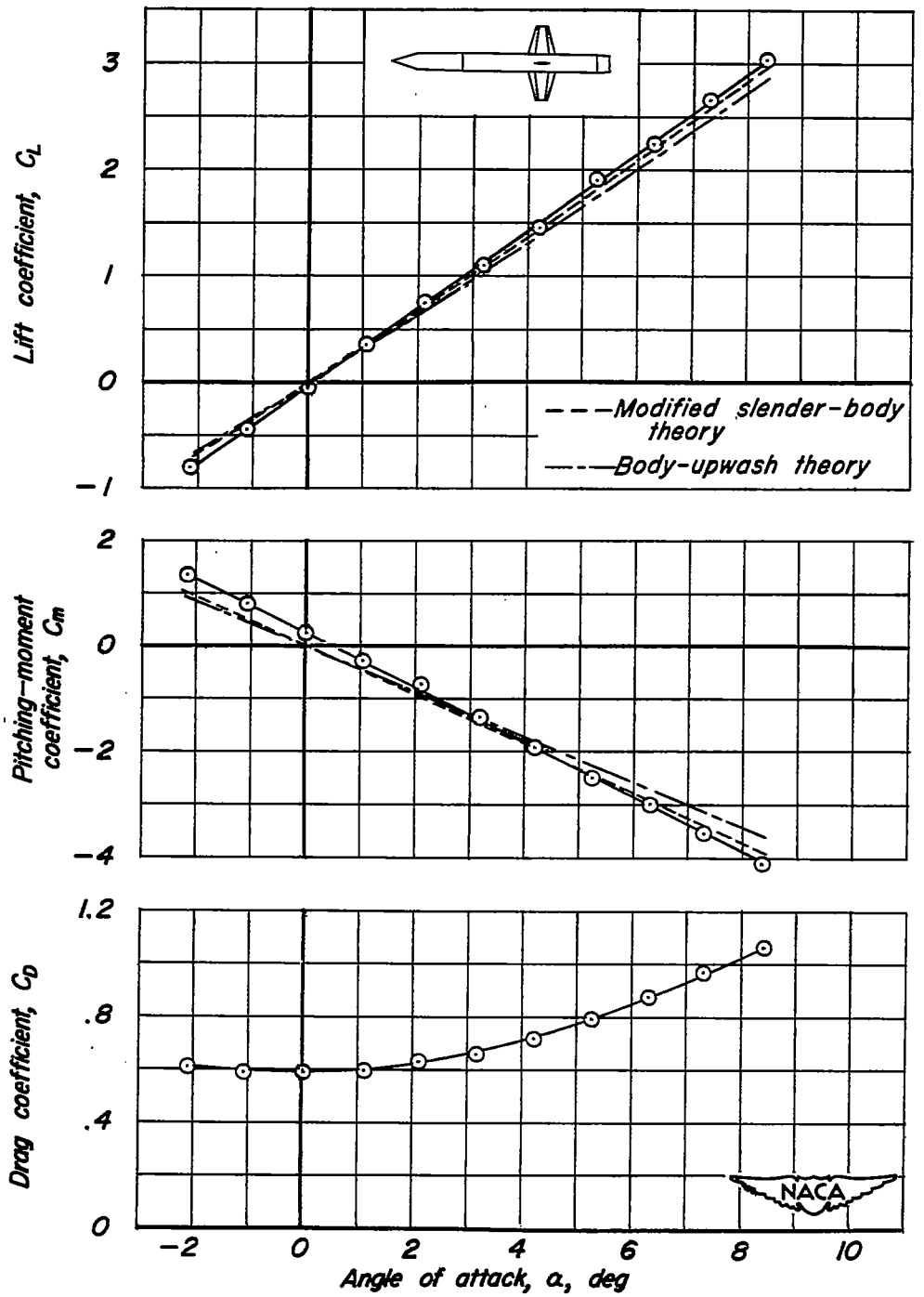

(a) M=1.5

Figure 7. —Variation of lift, pitching-moment, and drag cofficients with angle of attack, configuration BHV.

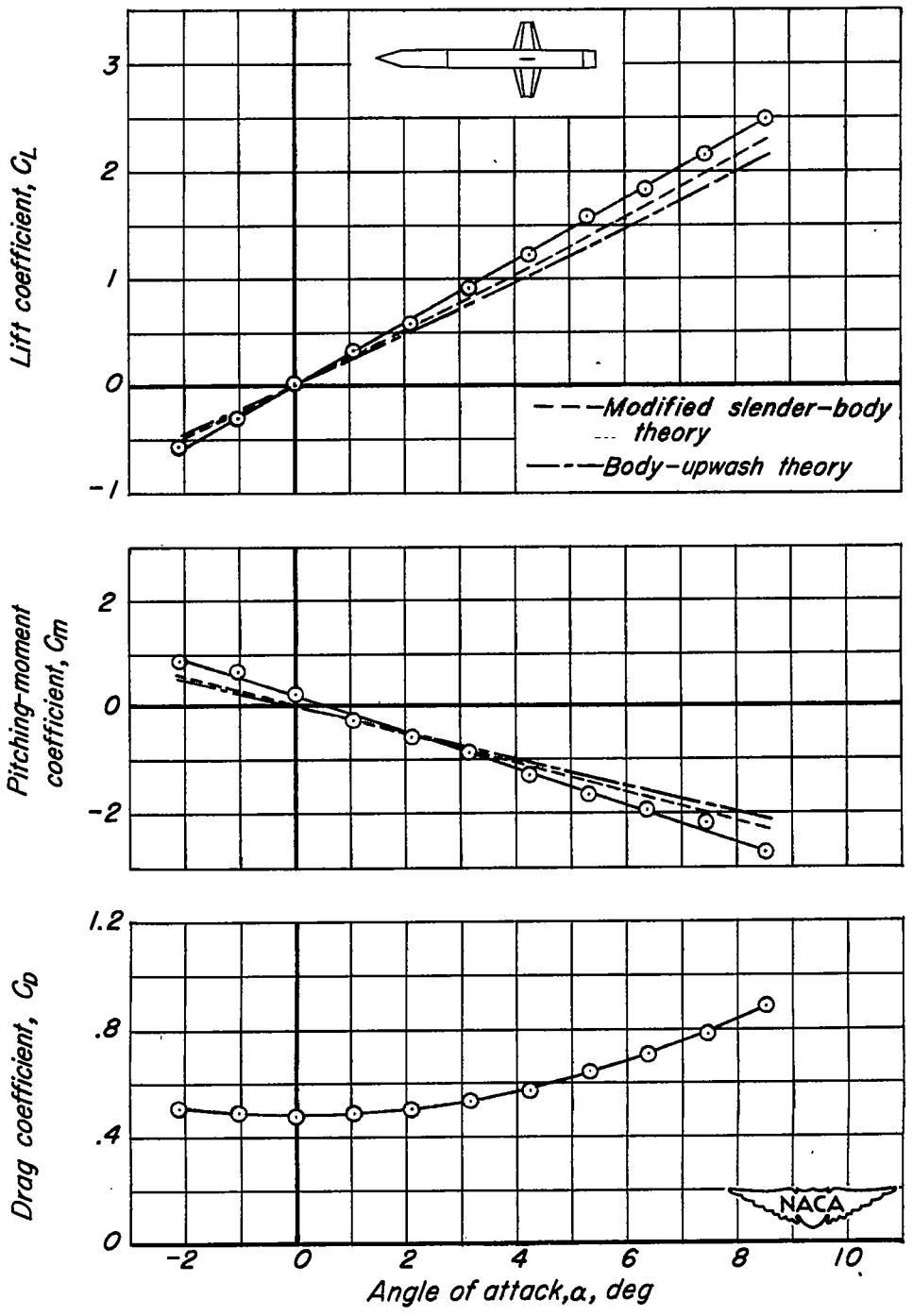

(b) $M = 2.0$

Figure 7. – Concluded.

[redacted]

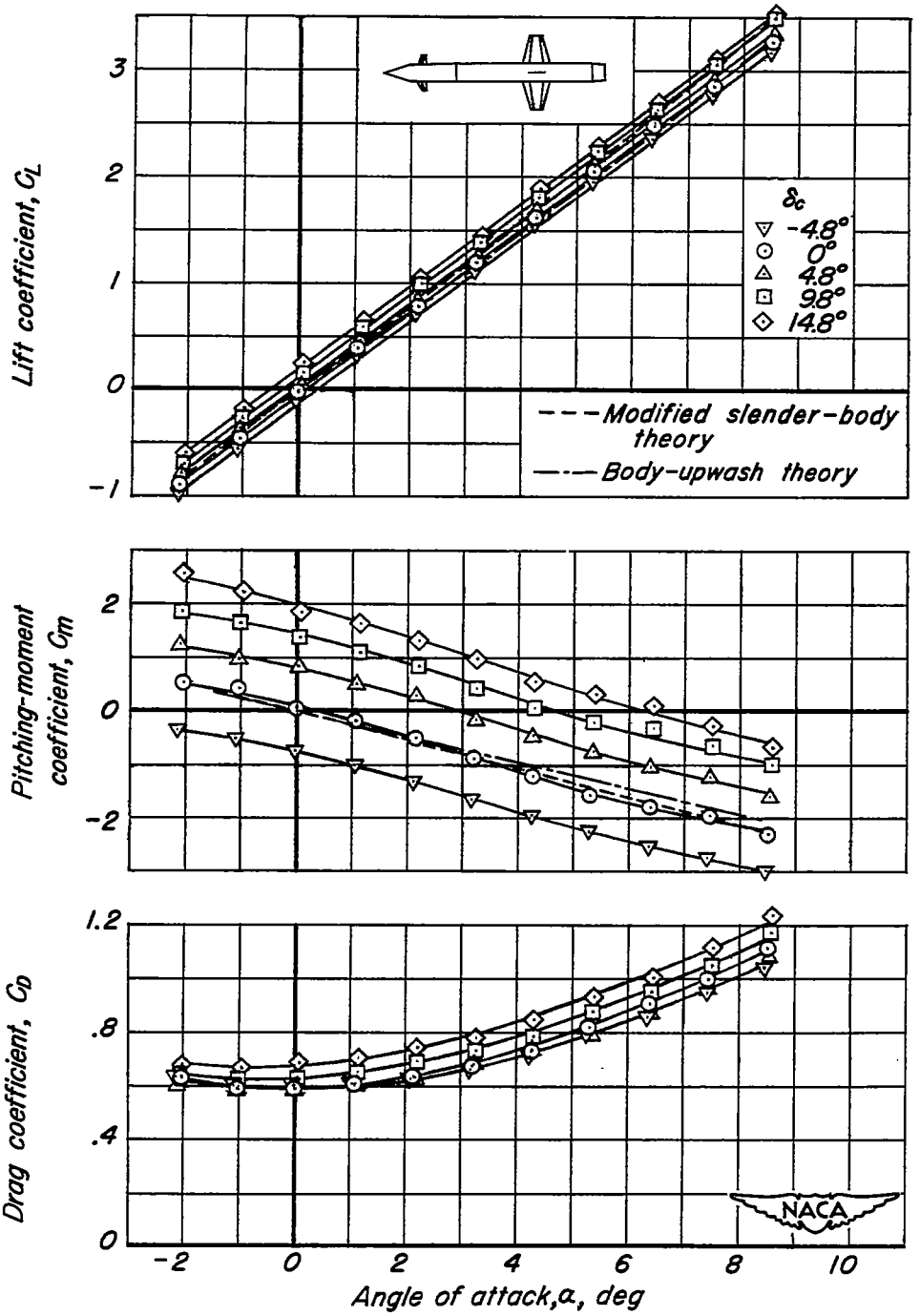

(a) $M = 1.5$

Figure 8.—Variation of lift, pitching-moment, and drag coefficients with angle of attack, configuration BHVC.

[redacted]

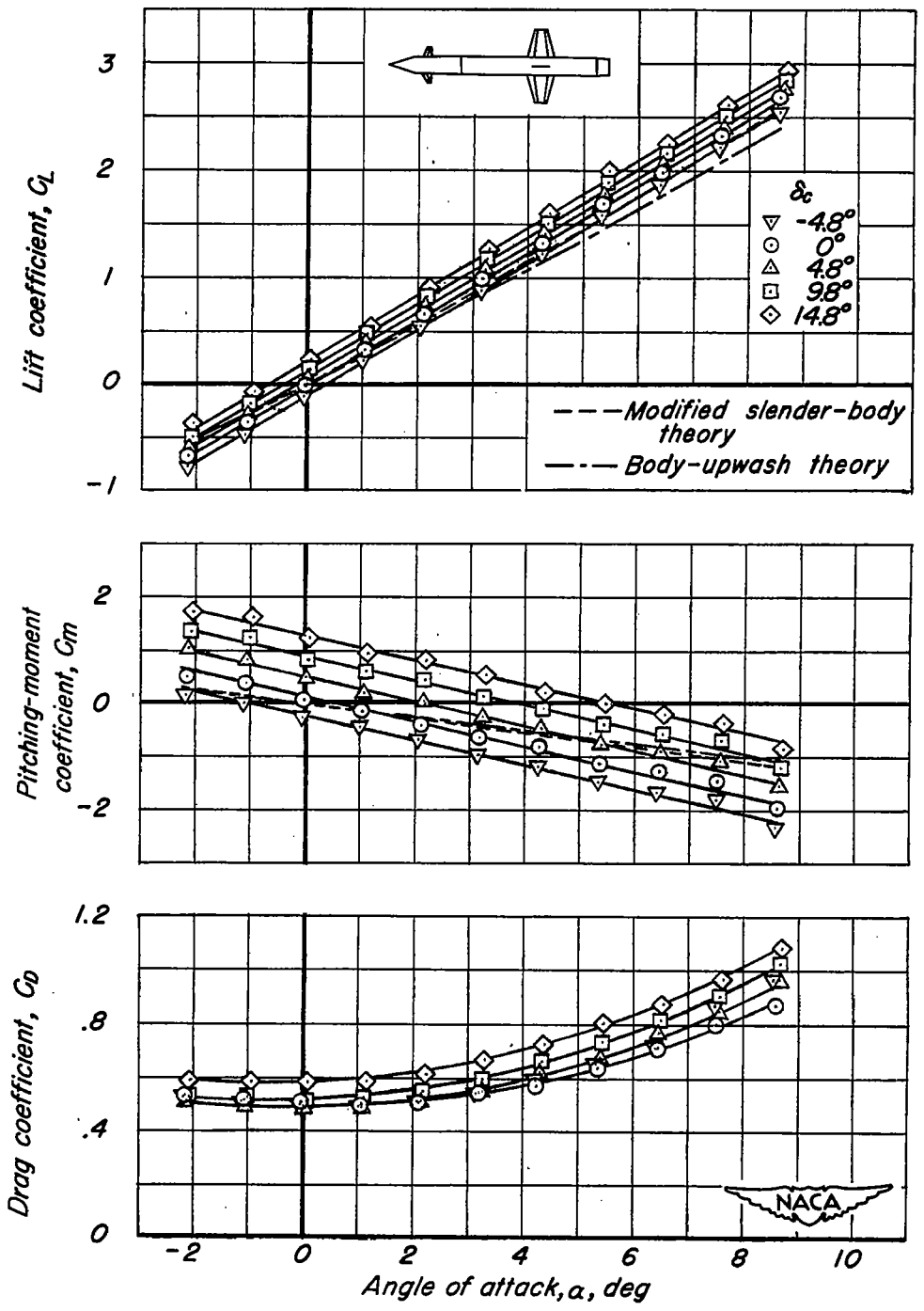

(b) M = 2.0

Figure 8.- Concluded.

[redacted]

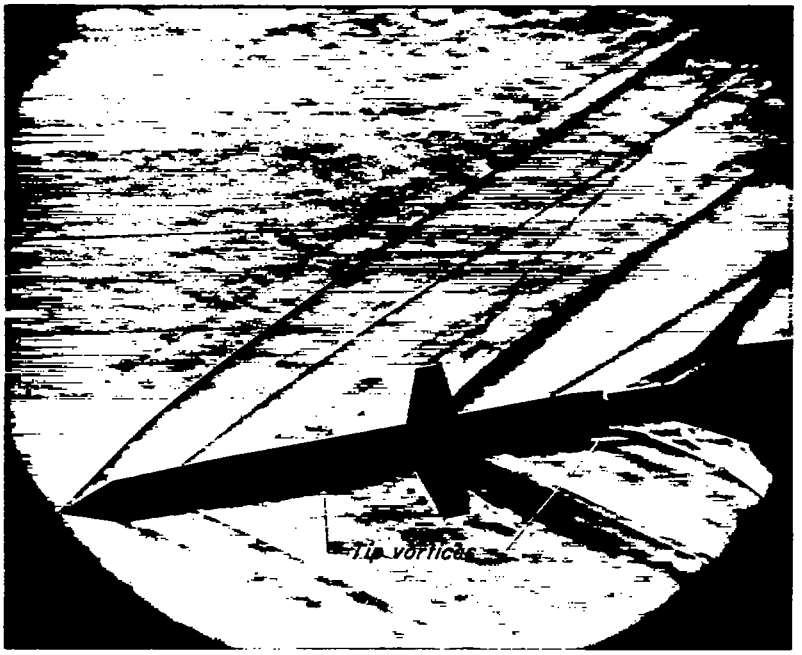

NACA
A-15305.1

(a) Side view, $\alpha = 8.6^{\circ}$.

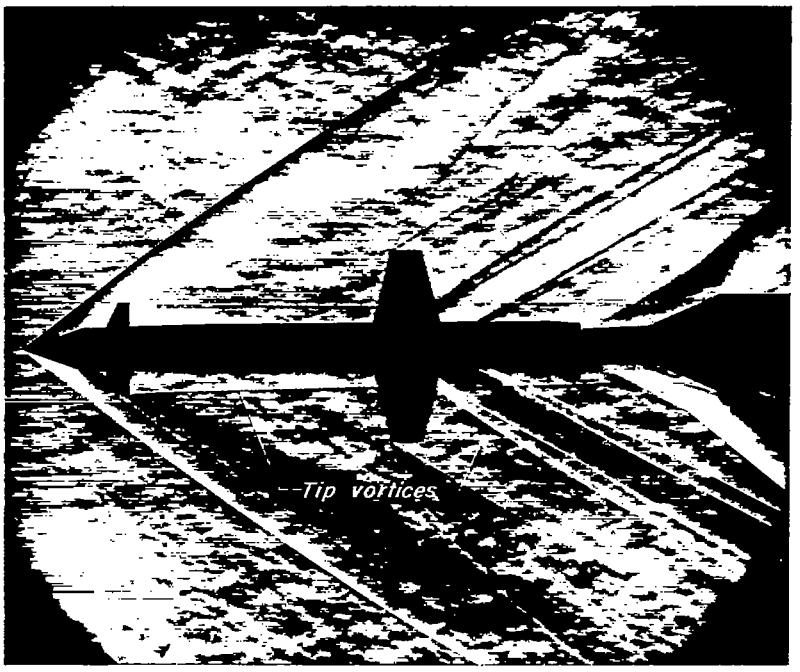

NACA
A-14270.1

(b) Plan view, $\alpha = 3^{\circ}$.

Figure 9.– Schlieren photographs of configuration BHVC in pitch, $\delta_c = 10^{\circ}$, M = 2.0.

[redacted]

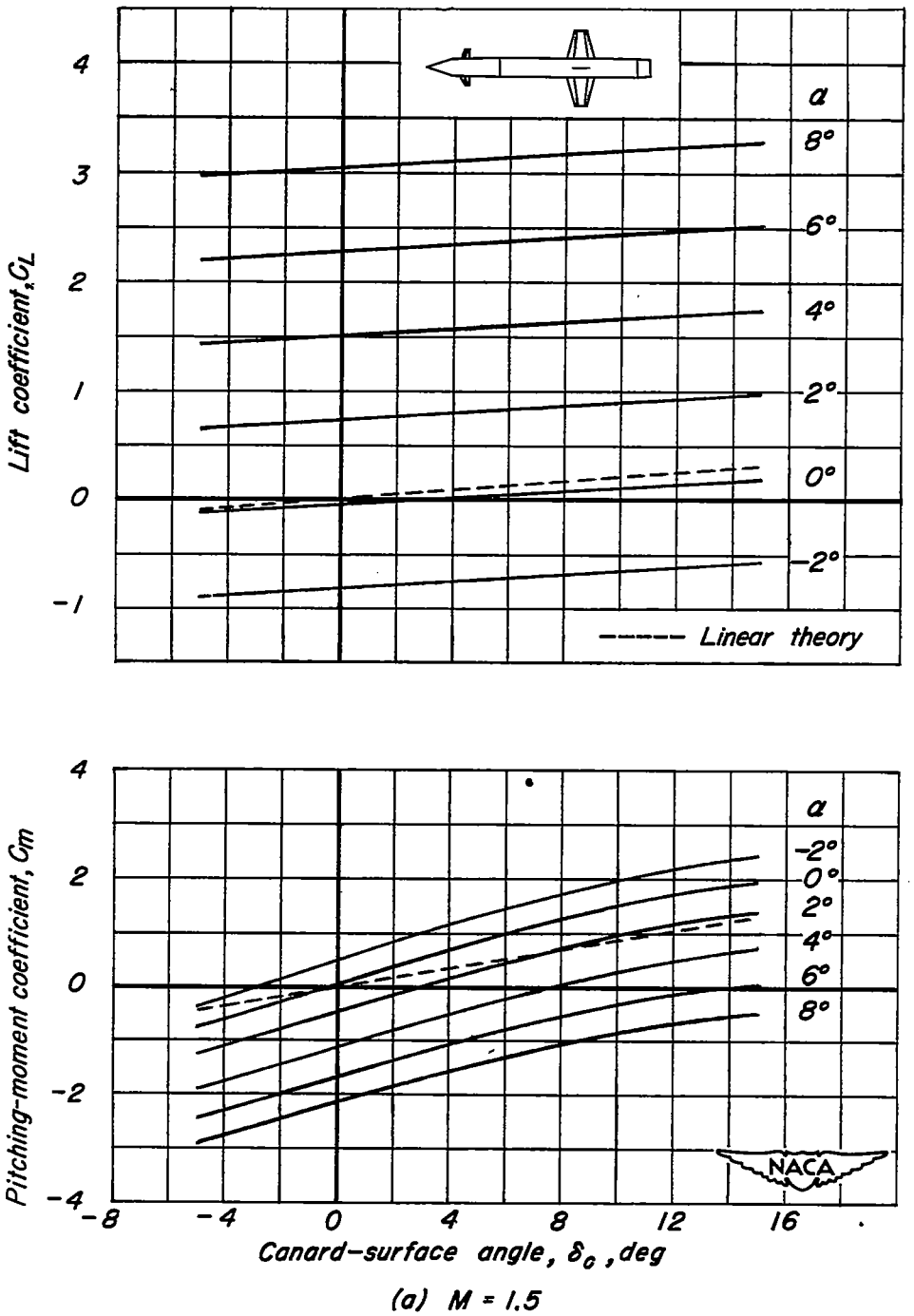

(a) M = 1.5

Figure 10.—Variation of lift and pitching-moment coefficients with canard-surface angle, configuration BHVC.

[redacted]

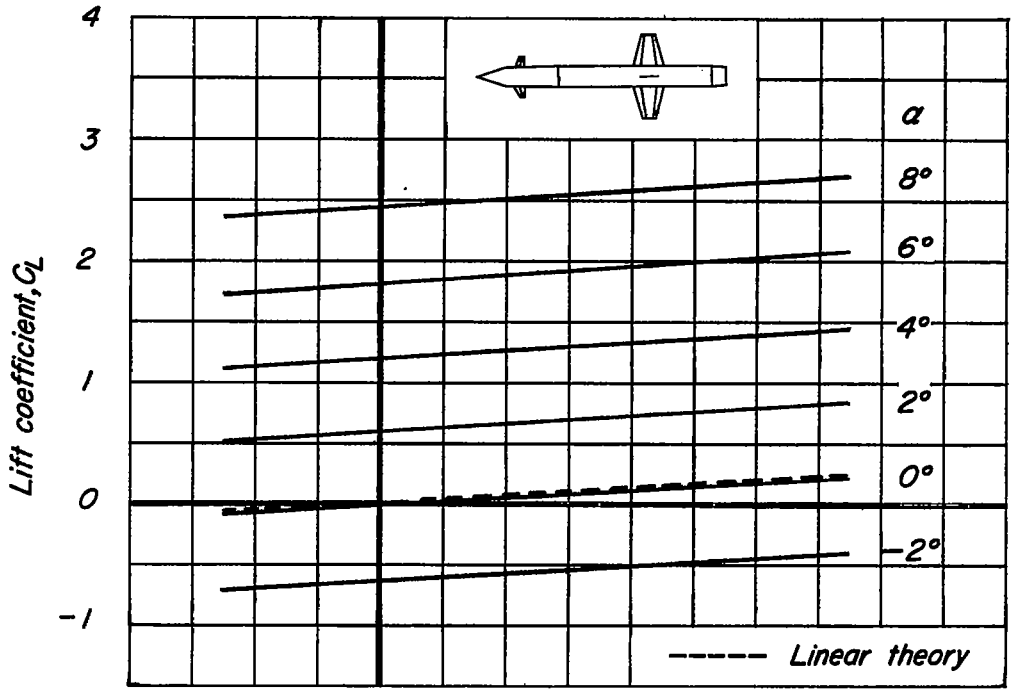

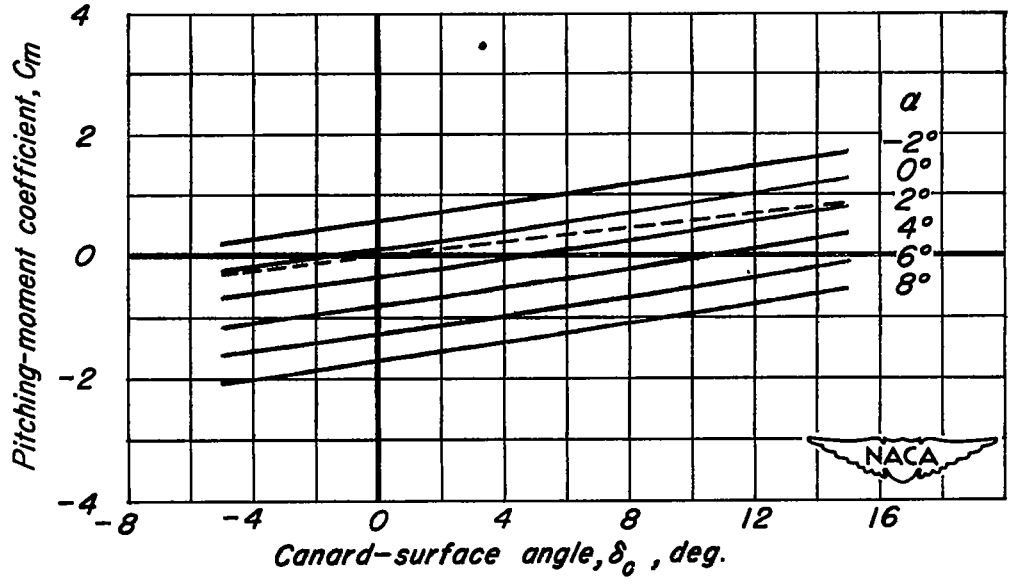

(b) M = 2.0

Figure 10.- Concluded.

[redacted]

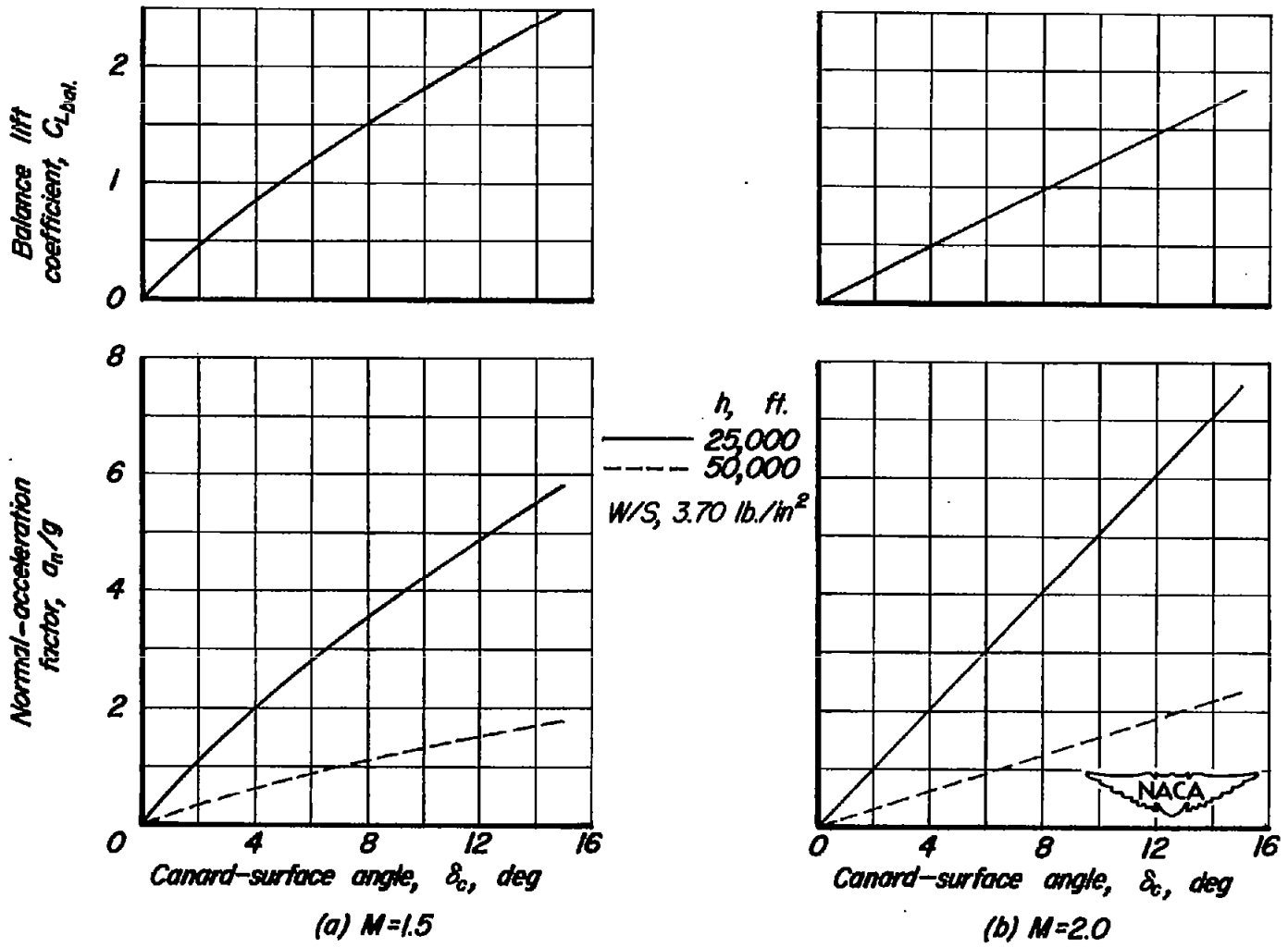

Figure 11.—Variation of balance lift coefficient and normal-acceleration factor with canard-surface angle, configuration BHVC.

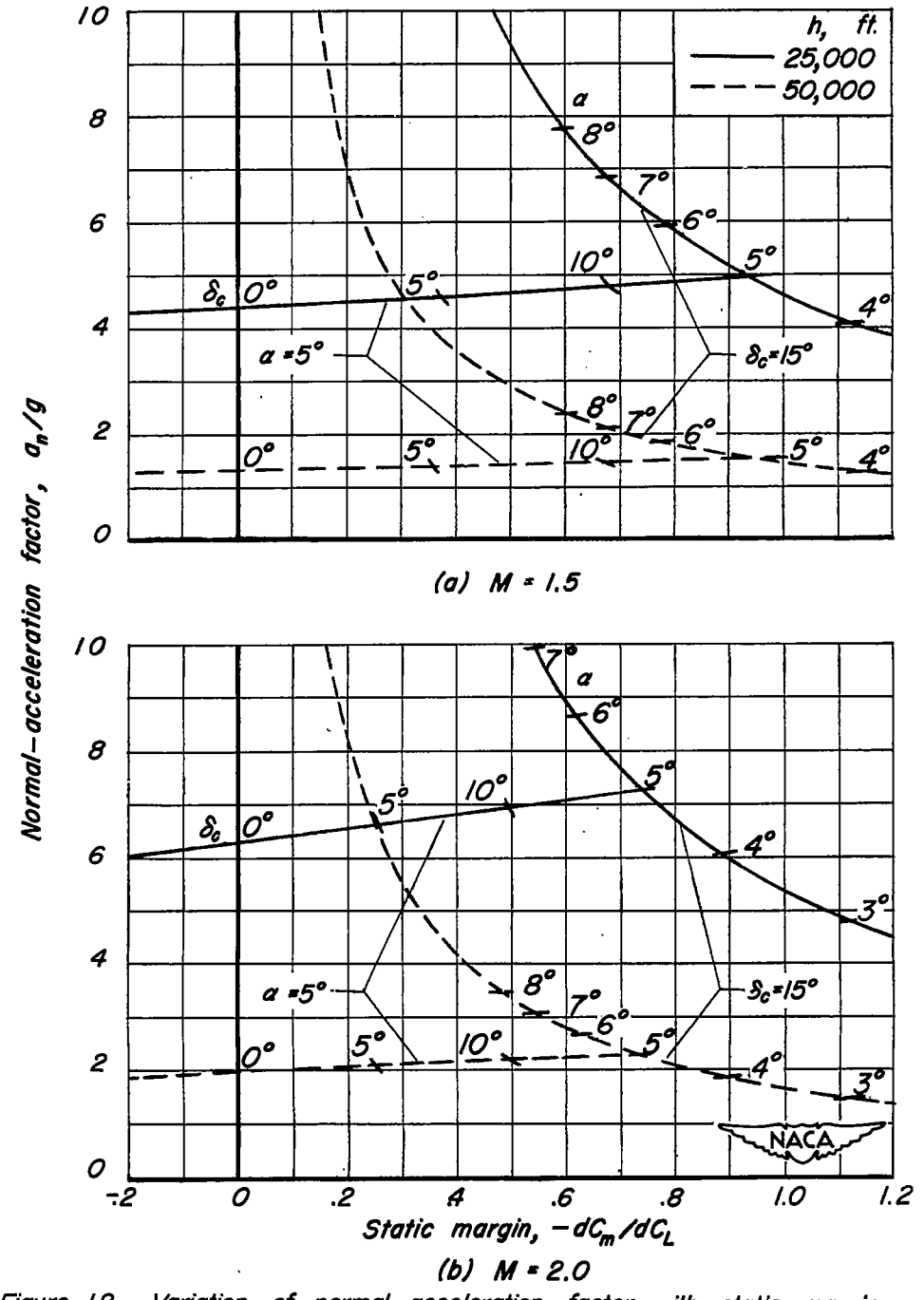

Figure 12.—Variation of normal-acceleration factor with static margin, configuration BHVC, W/S=3.70 lb./in.^{2}

[redacted]

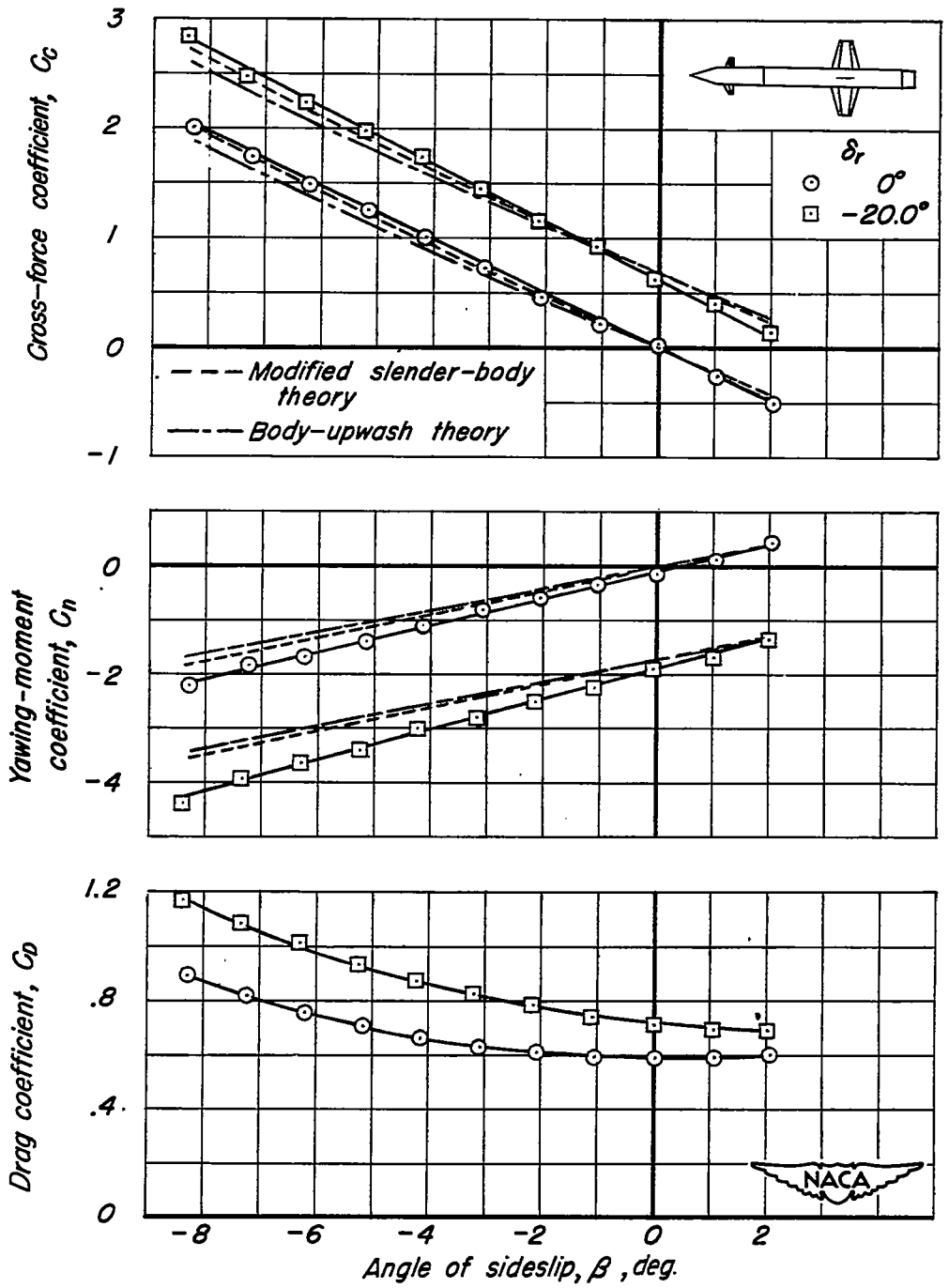

(a) $M = 1.5$

Figure 13.—Variation of cross-force, yawing-moment, and drag coefficients with angle of sideslip, configuration BHVC, $\alpha = 0°$.

[redacted]

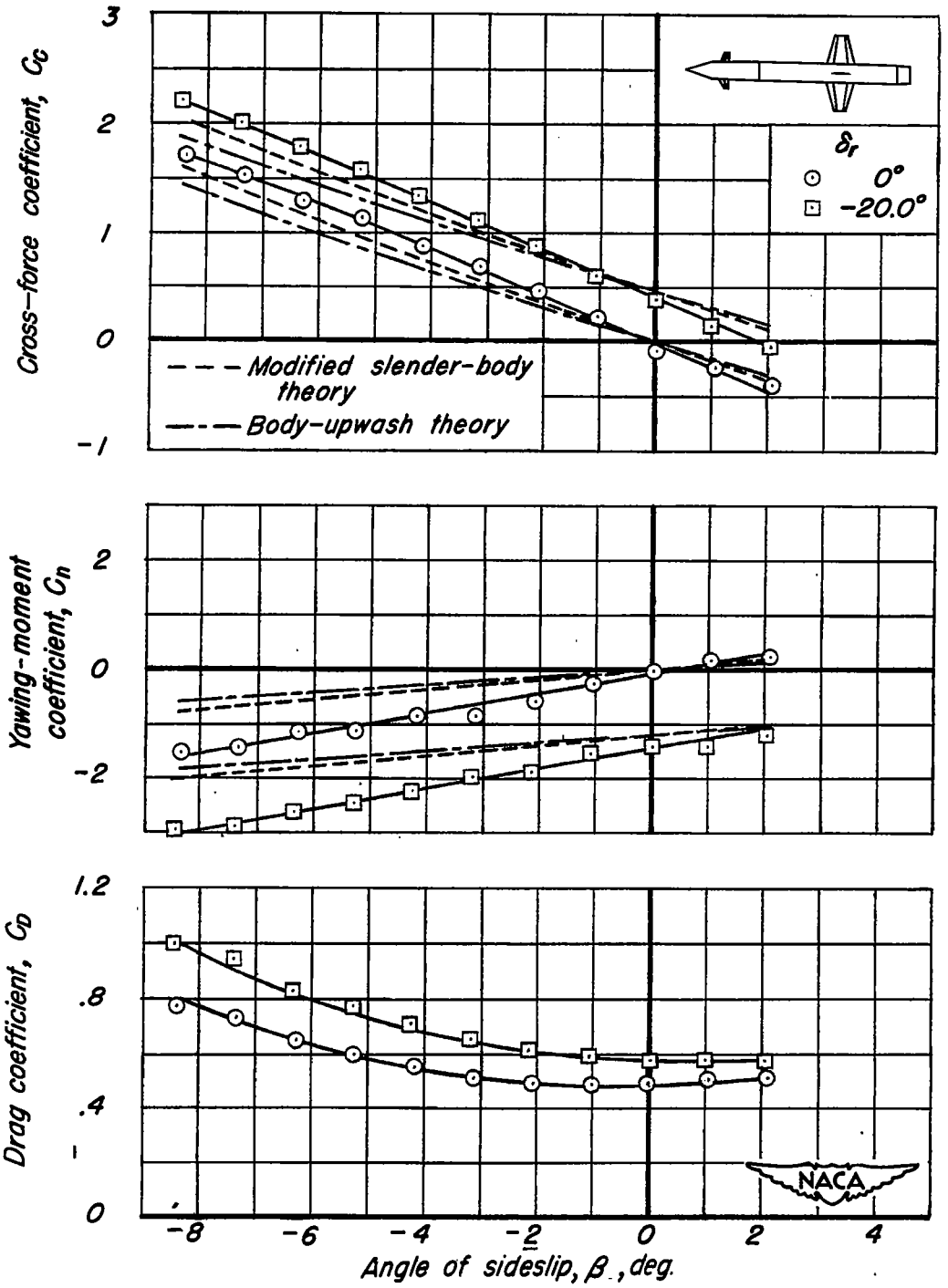

(b) M = 2.0

Figure 13.- Concluded.

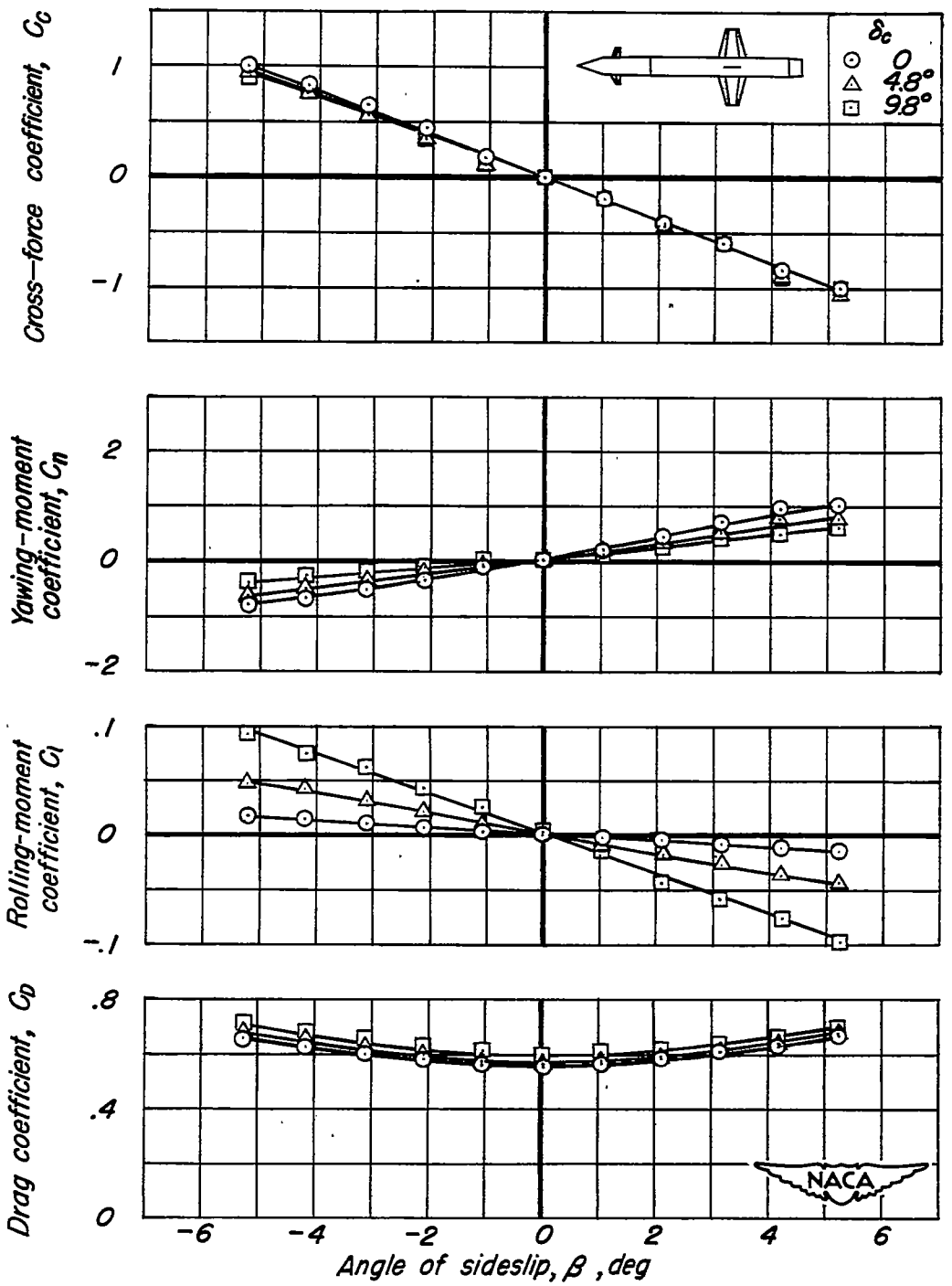

Figure 14.—Variation of cross-force, yawing-moment, rolling-moment, and drag coefficients with angle of sideslip, configuration BHVC, M=2.0, α=3°.

[redacted]